Ultrafast Heme Dynamics in Ferrous versus Ferric Cytochrome *c* Studied by Time-Resolved Resonance Raman and Transient Absorption Spectroscopy

Michel Negrerie,[†,‡] Simona Cianetti,[†,§] Marten H. Vos,[†,‡] Jean-Louis Martin,[†,‡] and Sergei G. Kruglik*[,†,||]

Laboratory for Optics and Biosciences, CNRS UMR 7645, Ecole Polytechnique, 91128 Palaiseau Cedex, France, INSERM Unité 696, 91128 Palaiseau Cedex, France, LENS, University of Florence, 50019 Sesto Fiorentino, Italy, and BioMoCeTi, CNRS UMR 7033, University Pierre & Marie Curie, Genopole Campus 1, 5 Rue Henri Desbrueres, 91030 Evry Cedex, France

Received: October 17, 2005; In Final Form: April 20, 2006

Cytochrome *c* (Cyt *c*) is a heme protein involved in electron transfer and also in apoptosis. Its heme iron is bisaxially ligated to histidine and methionine side chains and both ferric and ferrous redox states are physiologically relevant, as well as a ligand exchange between internal residue and external diatomic molecule. The photodissociation of internal axial ligand was observed for several ferrous heme proteins including Cyt *c*, but no time-resolved studies have been reported on ferric Cyt *c*. To investigate how the oxidation state of the heme influences the primary photoprocesses, we performed a comprehensive comparative study on horse heart Cyt *c* by subpicosecond time-resolved resonance Raman and femtosecond transient absorption spectroscopy. We found that in ferric Cyt *c*, in contrast to ferrous Cyt *c*, the photodissociation of an internal ligand does not take place, and relaxation dynamics is dominated by vibrational cooling in the ground electronic state of the heme. The intermolecular vibrational energy transfer was found to proceed in a single phase with a temperature decay of ∼7 ps in both ferric and ferrous Cyt *c*. For ferrous Cyt *c*, the instantaneous photodissociation of the methionine side chain from the heme iron is the dominant event, and its rebinding proceeds in two phases, with time constants of ∼5 and ∼16 ps. A mechanism of this process is discussed, and the difference in photoinduced coordination behavior between ferric and ferrous Cyt *c* is explained by an involvement of the excited electronic state coupled with conformational relaxation of the heme.

Introduction

Cytochrome *c* (Cyt *c*) is a redox-active protein involved in a wide variety of biological processes.[1,2] In native Cyt *c*, the heme iron is ligated to the protein backbone via two axial bonds[3] involving a proximal[4] histidine (His-18) and a distal methionine (Met-80) internal residues and can adopt ferric (Fe^{3+}) and ferrous (Fe^{2+}) oxidation states. Both proximal and distal heme-iron coordination bonds are crucial for protein functioning. In most heme proteins, the binding and release kinetics of diatomic ligands depend on the coordination state and the redox state of the heme iron, which are themselves involved in the triggering of catalytic activity.[5] In some cases, even if the heme iron is coordinated at both axial positions by amino acid residues, an exogenous diatomic ligand can displace one of them and bind to the iron, as observed in the sensor proteins CooA[6,7] and Dos[8,9] which bind CO and O_2, respectively. In other proteins, binding of NO induces the proximal bond cleavage, as in the case of the soluble guanylate cyclase[10,11] and eIF2α kinase.[12] Here, the binding of the diatomic ligand regulates enzymatic activity of these heme proteins.

The binding of nitric oxide to Cyt *c* during a physiological process has been discovered only recently[13] by the involvement of nitrosylated Cyt *c* in apoptosis. Whereas CO reacts only with Cyt *c* if Met-80 has been chemically modified[14] or mutated,[15] the in vitro reactivity of Cyt *c* towards exogenous NO has long been observed for both oxidation states of the heme iron.[16,17] Since resting native Cyt *c* possesses a six-coordinate heme, the cleavage of one axial bond involving an internal residue is required, this process being physiologically relevant. To get insight into the mechanism of the Cyt *c* interaction with diatomic ligands, it is necessary to identify the nature of the side-chain involved in bond breaking and to probe the structural consequences of this cleavage.

Breaking of heme iron−axial ligand bond can often be brought about with high quantum yield by the absorption of a photon by the heme. This implies that the initial phases of the NO−internal residue exchange in Cyt *c* can be triggered by ultrashort light pulses from both sides. The results of time-resolved studies of the coordination dynamics in the Cyt *c*−NO system will be presented elsewhere.[18] In this paper, we focus on the heme dynamics after photoexcitation of the native Met−Fe−His bound form.

Femtosecond optical spectroscopy provides a unique possibility to study the ultrafast heme structural dynamics.[19] After absorption of the pump pulse by the heme, a bond breaking event is triggered, and the subsequent ultrafast dynamics can be followed by the delayed probe pulse. Previous studies on ferrous Cyt *c* based on femtosecond transient absorption (TA) technique with excitation in the δ-band (314 nm)[20] and in the Soret band (400 nm)[21] of the heme contrarily suggested the photolysis of His-18 and Met-80 internal residues, respectively. The observed relaxation kinetics in both experiments[20,21] were

* To whom correspondence should be addressed. E-mail: kruglik@ccr.jussieu.fr.
† CNRS, Ecole Polytechnique.
‡ INSERM.
§ University of Florence.
|| CNRS, University Pierre & Marie Curie.

10.1021/jp0559377 CCC: $33.50
Published on Web 06/02/2006

found to be extremely fast, with an axial-ligand rebinding time constant of about 6 ps: that is on the time scale of electronic and vibrational relaxation of photoexcited heme.[19−32] Therefore, for ferrous Cyt *c*, the photoproduct TA spectra contain simultaneous contributions from different relaxation processes, complicating spectral interpretation.

Along with TA, femtosecond coherence spectroscopy of ferrous Cyt *c* has been performed,[21] and the vibrational modes of the photoproduct at ∼40, ∼80, and ∼220 cm^{-1} have been reconstructed from coherent oscillations and interpreted as a manifestation of Met-80 detachment rather than His-18.

Complimentary to TA, time-resolved resonance Raman (TR^3) is a direct structure-sensitive tool for studying the processes of energy relaxation and coordination dynamics in heme proteins and heme model compounds.[24,33−48] For the six-coordinate heme iron, the photodissociation of one axial ligand results in a five-coordinate transient domed structure with a subsequent motion of the central metal out of the heme plane[35,39,40] inducing a change in Raman activity for some low-frequency modes, in particular of the Fe−His stretch, located in the 200−250 cm^{-1} range.[49] In the high-frequency region, pronounced frequency shifts of porphyrin marker bands take place as a result of heme coordination and spin-state changes.[50] TR^3 spectroscopy is therefore a tool of choice for monitoring the dynamics of heme coordination state and for investigating other localized perturbations coupled to the iron out-of-plane motion.

Recently, in a short communication,[51] we have unequivocally demonstrated from TR^3 spectra in the low-frequency range that the distal Met-80 residue is photodissociated from the heme of ferrous Cyt *c* upon excitation in the α−band at 550 nm, and His-18 is not. The frequency of the Fe−His mode was found at 216 cm^{-1} for the five-coordinate transient ferrous Cyt *c* species. In the present full paper, Cyt *c* photoinduced dynamics is studied in detail by the combined use of subpicosecond TR^3 and femtosecond TA spectroscopy. TR^3 spectroscopy allowed monitoring of time-dependent photoinduced structural changes as well as vibrational heating, while TA spectroscopy was used for the determination of kinetic time constants, and to monitor the changes in electronic structure of the heme.

To evaluate the role of the protein structure, we investigate also a model ferrous Cyt *c* fragment[52] having N-terminal residues 1−56 (hereafter referred to as N-fragment). This N-fragment contains the heme covalently bound to the polypeptide chain as in native Cyt *c*, but lacks the C-terminal chain so that no ordered secondary structure is evident.[52] Since the Cyt *c* N-fragment, at pH 9, possesses a heme group axially bound to two histidine residues,[53] it was also used as a model of Fe−His bond photocleavage.

By now, to the best of our knowledge, no time-resolved studies have been reported on the primary photoprocesses in Cyt *c* in its ferric oxidation state. Photodissociation of axial ligands has been observed for many ferrous heme proteins, while ferric hemes appear to be more photoinert with respect to the iron-axial ligand bond. However, photodissociation of 1-methylimidazole from model ferric iron porphyrin has been reported recently.[54] To investigate how the oxidation state of the heme influences the primary photoprocesses, we performed detailed comparative TR^3 and TA measurements of the ferrous and ferric species of horse heart Cyt *c*, measuring contributions from the excited states deactivation, vibrational and conformational relaxations, and evolution of the heme coordination state. One important conclusion is that photodissociation of axial ligands does not occur from the ferric heme.

Experimental Section

Sample Preparation. Horse heart Cyt *c* was purchased from Sigma Chemical. Ferric Cyt *c* was prepared by purification of the commercial protein onto a Sepharose G-25 column (Amersham Biosciences) previously equilibrated with the 0.1 M Tris/HCl buffer (pH 7.4), using an Akta Purifier FPLC system (Amersham Biosciences). No oxidant was added to the solution of ferric Cyt *c*. Ferrous Cyt *c* was prepared by anaerobically reducing ferric Cyt *c* in pH 7.4 buffer using 1 mM sodium dithionite or dithiotreitol.

The Cyt *c* N-fragment (residues 1−56) was obtained by limited proteolysis of the native protein.[52] The ferrous N-fragment was prepared by reducing the ferric form in 0.1 M Tris/HCl buffer (pH 9) with 1 mM sodium dithionite.

The concentration of all samples during TA measurements was adjusted to 125 μM which corresponds to optical density (OD) = 1.25 and 1.5 at the Soret maximum (optical path length, 1 mm) for the oxidized and reduced forms of Cyt *c*, respectively. For Raman measurements, the protein concentration was adjusted to 300 μM, and ammonium sulfate (0.5 M) was added in the solution for Raman intensity calibration.

All experiments were carried out at room temperature. The absorption spectra of the samples were verified before and after time-resolved experiments using a Shimadzu 1601 spectrophotometer.

Femtosecond TA Spectra and Kinetics. The femtosecond TA spectrometer, described in detail elsewhere,[19] operated at 30 Hz and provided excitation pulses (∼0.1 μJ centered around 550 nm) and white light continuum probe pulses of about 50 fs duration. Both beams were focused to a spot of ∼50 μm and spatially overlapped in the sample cell, which was continuously moved perpendicular to the beams to ensure sample renewal between the shots. For each laser shot, a reference probe intensity was measured simultaneously with the probe intensity passing through the sample in order to calculate the absorbance change. The TA spectra were registered with a polychromator coupled to a CCD camera, and up to 900 spectra at each time point were averaged.

The group velocity dispersion (GVD) of the probe white-light pulse was compensated by a set of prisms. We tuned the minimum of GVD curve to ∼ 415 nm, at the center of the spectral range of interest, and we restrained data analysis to the range 385−445 nm. As a result, the remaining temporal distortion amounted to less than 0.2 ps over the entire analyzed spectral range, and the cross phase modulation artifact was negligible or small, so that the global analysis of the data was accurate down to 0.3 ps, the shorter limit of the processes that we focus on in this study.

Subpicosecond TR^3 Spectra. A novel subpicosecond Raman spectrometer has been developed[51] which will be described in detail elsewhere. Briefly, a homemade femtosecond Ti:Sapphire oscillator[55] was pumped by a solid-state diode-pumped laser (Spectra Physics, Millenia) producing ∼50 fs pulses with a repetition rate of 80 MHz. The seed pulse from this laser was amplified in a regenerative amplifier (Positive Light, Spitfire) pumped by a frequency-doubled Nd:YLF laser (Spectra Physics, Merlin). The output radiation from the regenerative amplifier after the compression stage had an energy of ∼0.6 mJ at 810 nm, and the repetition rate was 1 kHz.

The second harmonic radiation (λ = 405 nm) produced in BBO crystals was used to feed the dual-channel pump−probe tunable optical part based on a home-built optical parametric generator and two noncollinearly phase-matched optical parametric amplifiers, also utilizing BBO crystals. In the pump

channel, the energy of the pulse with ≤100 fs duration was 1.7−2.3 μJ in a sample cell, and the excitation was centered at 550 nm. In the probe channel, the radiation at 870 nm after amplification was doubled in a BBO crystal to produce a Raman probe at 435 nm. Then, this probe light passed through a specially designed narrowband interference filter (Barr Associates) to achieve the best compromise between spectral (30 cm^{-1}, fwhm) and temporal (0.63 ± 0.04 ps, Gaussian fit) resolutions in time-resolved Raman measurements. The probe pulse energy was 20−30 nJ in the sample cell. Pump and probe beams were collinearly superimposed by a dichroic mirror and focused on the sample by a spherical lens with $f = 10$ cm. Raman spectra were recorded using a 90° light-collection geometry with excitation from the bottom of the cell. Polarizations of pump and probe beams were set parallel to each other since protein reorientation is negligible in the time range studied. The focused pump beam spot on the bottom of the cell had a diameter of 130−150 μm (fwhm), while the probe beam spot was slightly asymmetrical with the diameters of ∼40 μm and ∼50 μm in the orthogonal axes. The optical delay time (Δt) between the pump and the probe pulses was controlled by a motorized translation stage (Newport M-ILS250PP). The instrumental time response function in pump−probe configuration was measured before each TR^3 experiment from absorption changes in copper-(II)-octaethylporphyrin in benzene; the accuracy in determination of the point $\Delta t = 0$ was better than 0.2 ps.

The samples were placed in a standard five-window 1 cm UV-quartz cuvette (Hellma) containing a small stirring magnetic bar which ensures the exchange of the illuminated volume. Raman scattering light was collected by a camera lens (Leica Noctiflux-M) onto a 1 m spectrograph (Jobin-Yvon HR1000, 1200 mm^{-1} grating, slit width 0.4 mm) and registered by a liquid nitrogen-cooled CCD (Roper Scientific Spec-10:100B). Parasitic background due to strong pump light was rejected using two short-pass filters (Melles-Griot). Rayleigh scattering during the low-frequency measurements was rejected by specially designed sharp-edge long-pass filter (Barr Associates).

Raman frequency calibration was performed using Kr and Xe spectral lamps (Oriel) with an absolute accuracy of ±2 cm^{-1} and relative accuracy better than 1 cm^{-1}. Raman intensity normalization was made using the 980 cm^{-1} stretch of ammonium sulfate added to the buffer solution.

Steady-state resonance Raman spectra were recorded using a He−Cd laser with continuous wave (cw) excitation at 441.6 nm (∼4 mW) and a Jobin-Yvon T64000 Raman spectrometer.

Results

1. Stationary Absorption Spectra. Figure 1 presents steady-state absorption spectra of ferrous (a) and ferric (b) Cyt *c*, and its ferrous N-fragment (c), normalized for the same concentration. The Soret bands of Cyt *c* are blue-shifted with respect to another Met−Fe−His bis-ligated hemoprotein Dos[8,9] reflecting the impact of the covalent binding of the heme vinyl groups to cysteines on the electronic properties of Cyt *c*. The ferrous N-fragment at pH 9 has a spectrum very similar to that of the full-length Cyt *c*, but its Soret band is somewhat narrower and its maximum is red-shifted by 2 nm. At this pH, the fragment is predominantly six-coordinate low-spin (6cLS)[53] and its absorption spectrum is almost identical to those observed for bisHis cytochromes such as Cyt c_3[53] showing only very small five-coordinate high-spin (5cHS) form contribution (Figure 1c). In our study, we employed the N-fragment, namely, at pH 9 for comparison with the native 6cLS ferrous Cyt *c*.

For time-resolved measurements, hemes were excited at the maximum of the Q_{0-0} band, the lowest-lying electronic transition, minimizing the excess energy deposited into the heme. Both TR^3 and TA probe beams were located in the Soret band region, as indicated in Figure 1.

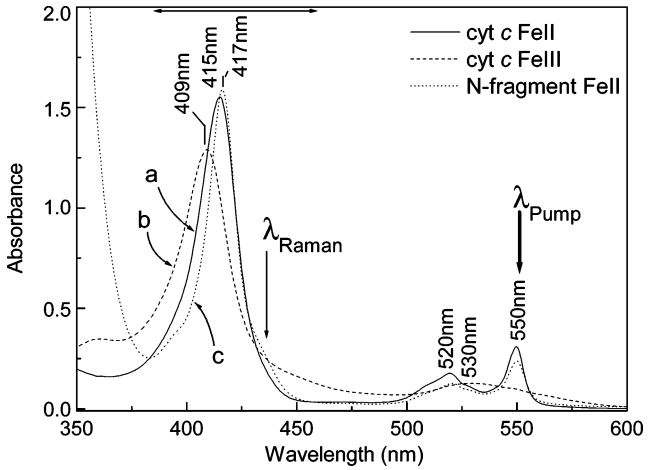

Figure 1. Absorption spectra of ferrous (a) and ferric (b) Cyt *c* at pH 7.4 and ferrous Cyt *c* N-fragment at pH 9.0 (c). The spectral range probed in the TA experiments is indicated by the horizontal arrow at the top. Pump and probe wavelengths in TR^3 experiments are indicated by the vertical arrows.

2. TA Data. *Ferrous Cyt c.* Figure 2 presents differential TA spectra of ferrous Cyt *c*, recorded at various delay times between pump and probe pulses (panel A), together with the results of singular value decomposition (SVD) analysis[56] and a fit to multiexponential functions (panels B−F). The TA spectra are dominated by the strong bleaching of the ground-state Soret band centered at ∼415 nm and a broad induced absorption extending beyond 440 nm (Figure 2A). Both the induced absorption maximum (∼428 nm at 1 ps) and the isosbestic point (∼422 nm at 0.66 ps) gradually shift to the blue by ∼3 nm during the first ∼10 ps (Figure 1S of Supporting Information). After 25 ps, ∼95% of the initial amplitude has decayed, and at 100 ps the ground state is completely recovered.

For SVD analysis, which allows us to extract global kinetic and spectral dependencies, the experimental data matrix $\Delta\mathbf{A}(\lambda, t)$ of differential TA spectra was decomposed according to

$$\Delta\mathbf{A}(\lambda, t) = \Delta\mathbf{A}^{SVD}(\lambda)\mathbf{S}\mathbf{K}^{SVD}(t) \quad (1)$$

giving the orthogonal spectral component matrix $\Delta\mathbf{A}^{SVD}(\lambda)$ and its associated kinetics matrix $\mathbf{K}^{SVD}(t)$ weighted according to the singular values S_i (elements of the diagonal matrix **S**).[57] This procedure allows separating the spectral components and their kinetic evolution within the data matrix and simultaneously suppressing the time-correlated noise components due to baseline fluctuations.

The singular values of the first 8 SVD components for ferrous Cyt *c* are presented in Figure 2B. Figures 2C and 2D show kinetics $\mathbf{K}^{SVD}(t)$ and spectra $\Delta\mathbf{A}^{SVD}(\lambda)$ corresponding to the major first three SVD components; amplitudes in panel 2D were scaled according to their singular values. It is clear that already the third SVD component is negligible, so it was not taken into account during further treatment. The kinetic components $K_j^{SVD}(t)$ were fitted to a multiexponential function

$$f(t) = \sum_i A_i \exp(-k_i t) \quad (2)$$

where the minimal number *i* of exponents was determined iteratively. In the case of ferrous Cyt *c*, four exponential

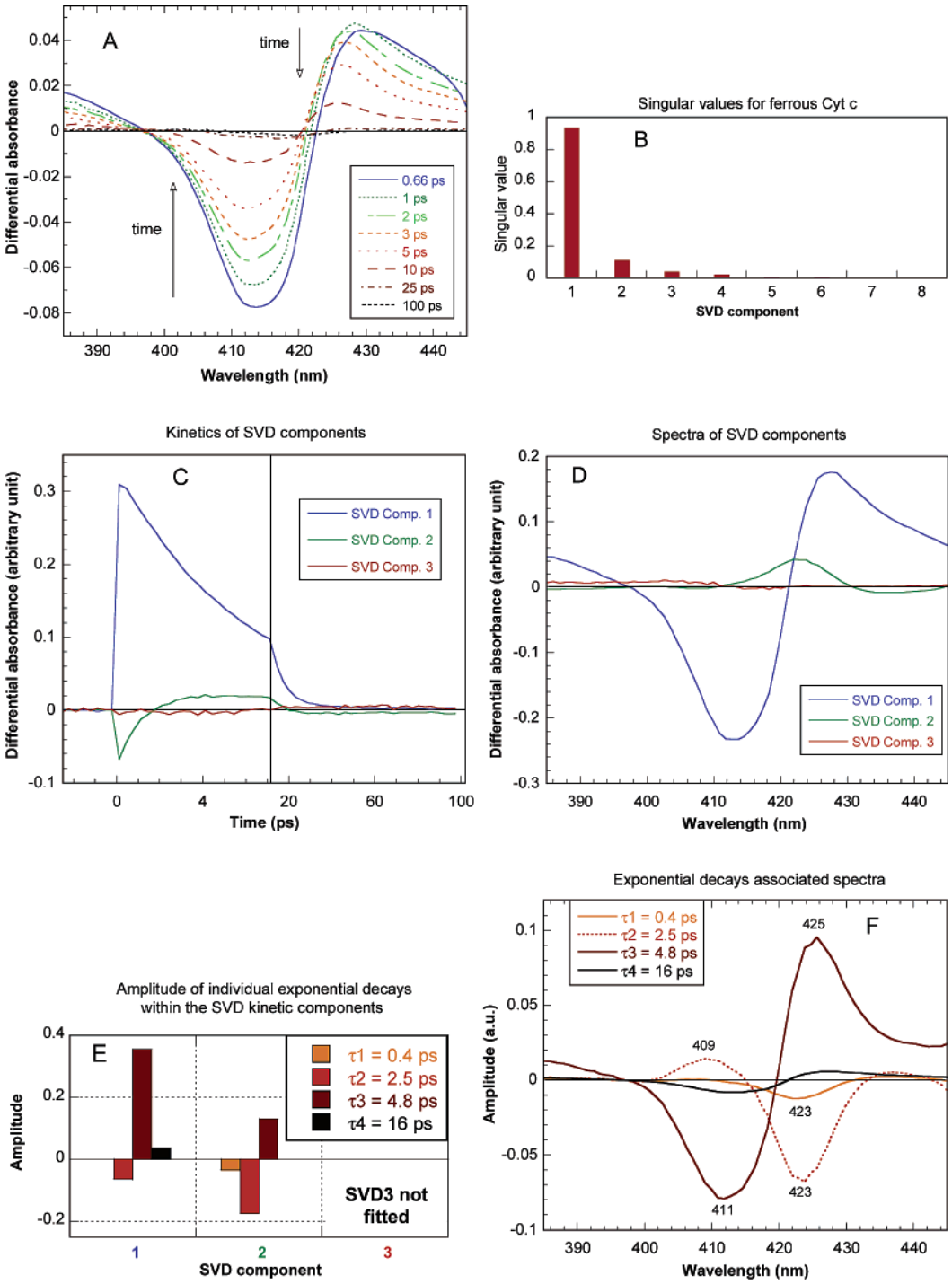

Figure 2. TA spectra of ferrous Cyt *c*, in buffer pH 7.4, shown at several chosen time delays (panel A) and the results of SVD analysis (panels B−D) and fits of these components in terms of DAS (E,F). See text for details of data treatment.

relaxation components were required to fit the data, with the decay time constants ($\tau_i = 1/k_i$) of ~0.4, 2.5, 4.8, and 16 ps. Including a nonzero asymptotic value did not improve the fit. The distribution of amplitudes of individual decays is presented in Figure 2E, the 4.8-ps process has a dominant contribution.

It is interesting to compare these relaxation times for ferrous Cyt *c* obtained by us using 550-nm excitation with those recently obtained in femtosecond TA study with 400-nm excitation,[21] where time constants of 0.1, 0.8, 2.8, and 6.2 ps were reported. Taking into account different excess energy deposited into the heme in these two experiments and keeping in mind that our analysis is accurate for $\Delta t \geq 0.3$ ps, the difference in fitted time constants <1 ps (0.4 ps versus 0.1 + 0.8 ps) is not surprising. The kinetic component of 2.5 ps in our experiment corresponds well to the 2.8-ps component in ref 21. Finally, the dominant relaxation of 6.2 ps reported previously[21] corresponds to 2 decays in our experiment, 4.8 ps (major contribution) and 16 ps (minor contribution), which we could separate because of the more extended time window. Note that when the number of components was restricted to 3 in eq 2, we have also found a longest relaxation time of about 6 ps, although the fit was not optimal in that case.

After optimizing the fit of the kinetic components, difference TA spectra associated with each monoexponential decay (decay

associated spectra, DAS) were calculated by

$$\mathrm{DAS}_i = \Sigma_j A_{i,j} S_j \Delta A_j^{\mathrm{SVD}}(\lambda) \quad (3)$$

where $A_{i,j}$ is the amplitude of the ith decay in the jth svd spectral component $\Delta A_j^{\mathrm{SVD}}(\lambda)$ whose singular value is S_j. In this way, every transient spectral species or process, characterized by its own DAS_i, presented in Figure 2F, was assigned to a particular relaxation time τ_i.

It is important to note that one of the relaxation processes involved is vibrational cooling, which, in general, is nonexponential[22] because the cooling rate depends on the temperature gradient between the locally hot heme and the ambient environment. Therefore, the obtained multiexponential kinetics should be considered as an approximative description of a more general nonexponential process. Moreover, we emphasize that this multiexponential fit does not necessarily represent a sequential decay model (see Discussion).

For ferrous Cyt *c*, the DAS corresponding to both τ_3 and τ_4 (Figure 2F) exhibit a characteristic derivative-like shape, but the positions of their isosbestic points are different: for DAS_4 (black line in Figure 2F), the isosbestic point is located around 422 nm and is red-shifted by ~3 nm with respect to that of DAS_3 (brown line), that is in the opposite direction to the general tendency of blue-shift observed during first ~10 ps (Figure 2A). This blue-shift is mathematically taken into account by the 2.8-ps DAS_2 which has roughly an opposite sign to the 4.8-ps DAS_3. Together these components thus describe a simultaneous blue shift and decay of a band, and we emphasize that in view of the simultaneousness of these processes an exponential decay model should only be considered as a convenient fit model for describing the spectral evolutions.

Ferrous N-Fragment. Figure 3 presents the TA data for the ferrous Cyt *c* N-fragment. In general, the evolution of the TA spectra of the N-fragment (Figure 3A) is qualitatively similar at early time delays to that of native Cyt *c* (Figure 2A), with the exception of a small red shift (few nm) of all spectral features due to the red-shifted ground-state Soret-band maximum (Figure 1a,c). However, longer time delays reveal a major difference: in the case of N-fragment, the transient absorption is still well detectable at 100 ps, and the ground state is not completely recovered even up to 1 ns (not shown).

The SVD-analysis of TA data for the ferrous Cyt *c* N-fragment revealed three major nonnegligible components (Figure 3B−D). Multiexponential fitting by eq 2 gave five global decays with time constants of 0.6, 2.7, 5.2, and 30 ps and a constant contribution, whose meaning is $\tau_5 \gg 1$ ns (Figure 3E). The first three time constants are reasonably similar to those of native Cyt *c*, whereas the kinetic behavior at longer time delays is different in the native protein and its truncated analogue. Corresponding DAS for N-fragment are presented in Figure 3F. The first four spectra are rather similar to those of native Cyt *c*, but the fifth DAS_5 ($\tau_5 \gg 1$ ns) is found only in the Cyt *c* N-fragment.

Again, as in the case of native Cyt *c*, $\mathrm{DAS}_{3,4,5}$ possess characteristic derivative-like shapes, and the isosbestic point of DAS_4 (solid black curve in Figure 3F) is red-shifted by ~3 nm with respect to DAS_3 (solid brown curve).

We also note a very interesting fact that DAS_5 (broken black curve), corresponding to the long-lived transient, has a very similar shape as DAS_4 and identical isosbestic points, thus corresponding to the evolution of the same transient species.

Ferric Cyt c. Figure 4 presents TA data for ferric Cyt *c*. The TA spectra (Figure 4A) are somewhat different from that of the ferrous heme (Figure 2A). For ferric Cyt *c* at early time delays, the spectra are dominated by a strong and broad bleaching ($\lambda_{\max}$ ~411 nm) slightly red-shifted with respect to the ground-state Soret-band maximum. This dominant bleaching quickly diminishes with time, and its maximum shifts to ~408 nm. The overall spectral pattern as well as the isosbestic point experiences a profound time-dependent blue shift (from 424 nm at 0.2 ps to about 414 nm at 6 ps, Figure 2S of Supporting Information), which is much more pronounced than in the case of ferrous Cyt *c*. Also, contrary to ferrous Cyt *c*, the induced absorption at 415−445 nm is weaker at early delay times.

All photoinduced processes in ferric Cyt *c* are very rapid: the differential absorbance totally vanishes already at 20 ps implying full recovery of the ground-state population. Importantly, we note the absence of a strong induced absorption for ferric Cyt *c* within the range 390−400 nm, to the blue of the ground-state Soret-band bleaching.

The SVD-analysis of the TA data revealed three major components (Figure 4B), their kinetics and spectra are presented in Figures 4C and 4D, correspondingly. Multiexponential fitting by eq 2 gave three global relaxation components: $\tau_1 < 0.3$ ps (the lower limit of our analysis), $\tau_2 = 0.9$ ps, and $\tau_3 = 4.2$ ps (Figure 4E). Global decay associated spectra are shown in Figure 4F: DAS_1 does not display any induced absorption within the reliable spectral zone of 395−425 nm but only a bleaching whose minimum is located at 415 nm. DAS_2 also does not disclose any induced absorption and is rather flat with a minor minimum located at 415−420 nm; that is in the range where the isosbestic point shifts. This component presumably reflects a decay along with a blue shift. DAS_3 displays a derivative-like shape and possesses a bleaching minimum at ~408 nm and an induced absorption maximum at ~422 nm.

However, as can be clearly seen from Figure 4A, the induced absorption maximum experiences a pronounced blue shift in the course of excitation relaxation, not a single maximum, presumably due to nonexponential vibrational relaxation processes.[31,32] Thus, the SVD analysis using multiexponential decay approximation describes this process by an average of time-dependent distributions of rates/states τ_2/DAS_2 and τ_3/DAS_3.

Again, we stress the difference in the photoinduced behavior between ferric and ferrous Cyt *c*: in the former case, relaxation dynamics is dominated by the τ_1 process associated with a spectral bleach (Figure 4E,F), while in the latter case a τ_3 process with derivative-like TA spectrum represents the major contribution (Figure 2E,F).

3. TR³ Data. *Ferrous Cyt c.* Figure 5 presents TR^3 spectra of ferrous Cyt *c* at pH 7.4, in the high-frequency region of the porphyrin marker bands.[50] Spectrum A is a steady-state spectrum measured with cw excitation at 441.6 nm representing scattering from the ground electronic state. This spectrum is consistent with a 6cLS metal configuration in ferrous Cyt *c* and is in agreement with literature data.[2,58] Spectrum B also represents the ground-state scattering, but with excitation at 435 nm by subpicosecond laser pulses, in a pump−probe configuration where the probe pulse arrived before the pump ($\Delta t = -5$ ps). Because of the decreased spectral resolution in time-resolved configuration, Raman lines in spectrum B are broader than in spectrum A. Nevertheless, both spectra are very similar, thus proving the absence of a perturbing influence of the subpicosecond probe beam, as well as the absence of an accumulated photoproduct with millisecond (or longer) lifetime because of the pump pulse arriving in the cell at a repetition rate of 1 kHz. Spectra C−L are difference TR^3 spectra, obtained after weighted subtraction of spectrum B, at various time delays between pump and probe pulses.

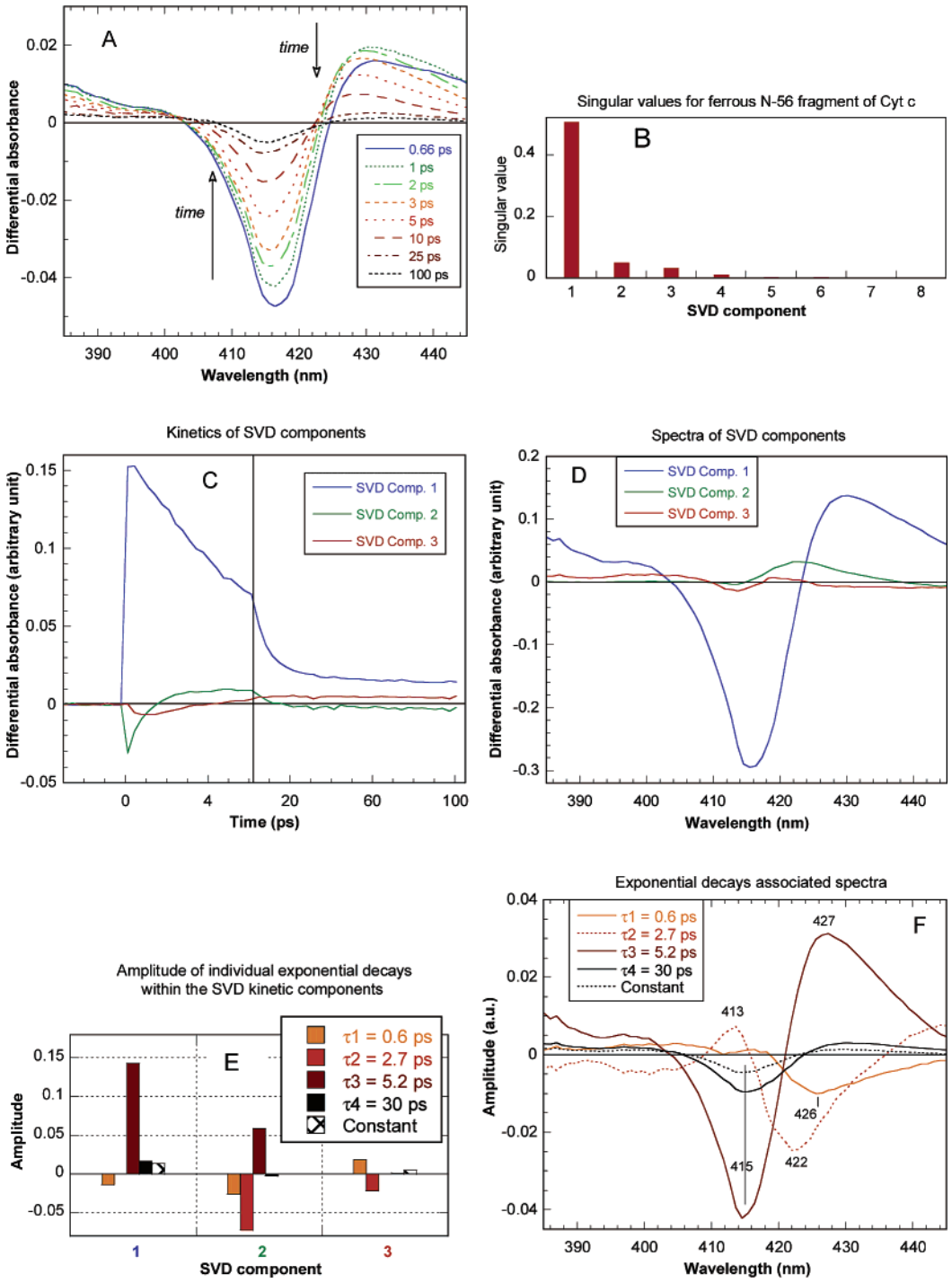

Figure 3. TA spectra of ferrous Cyt *c* N-fragment, in buffer pH 9, shown at several chosen time delays (panel A) and the results of SVD analysis (panels B−D) and fits of these components in terms of DAS (E,F). See text for details of data treatment.

In more detail, these difference spectra have been calculated from the experimentally measured ones using the following procedure. First, all measured TR^3 spectra have been corrected for both CCD dark current and parasitic background due to residual pump laser light penetrating into the spectrometer. In the low-frequency range, in addition, all spectra have been divided by the transmission curve of the rejection filters employed. After that, the remaining slowly changing background (if any, usually for low-frequency spectra) has been eliminated by subtracting an appropriate cubic spline function.

Second, the resulting spectra were normalized on the internal Raman intensity standard, 980 cm^{-1} line of SO_4^{2-}. This normalization procedure compensates for (i) power fluctuations of the probe beam with time, (ii) change of light reabsorption in the photoproduct states, as well as (iii) change of scattering volume (the depth of penetration of the probe beam) in the presence of the pump beam. Last, to obtain a pure photoproduct spectrum, a subtraction procedure has been implemented:

$$\text{Spectrum}(\Delta t)_{\text{difference}} = \text{Spectrum}(\Delta t)_{\text{normalized}} - K(\Delta t) \times \text{Spectrum}(-5\ \text{ps})_{\text{normalized}} \quad (4)$$

where the time-dependent factor $K(\Delta t)$ has been introduced at each time delay to suppress the contribution from the ground-state scattering. The choice of $K(\Delta t)$ can be made with good accuracy provided the photoproduct spectrum contains bands

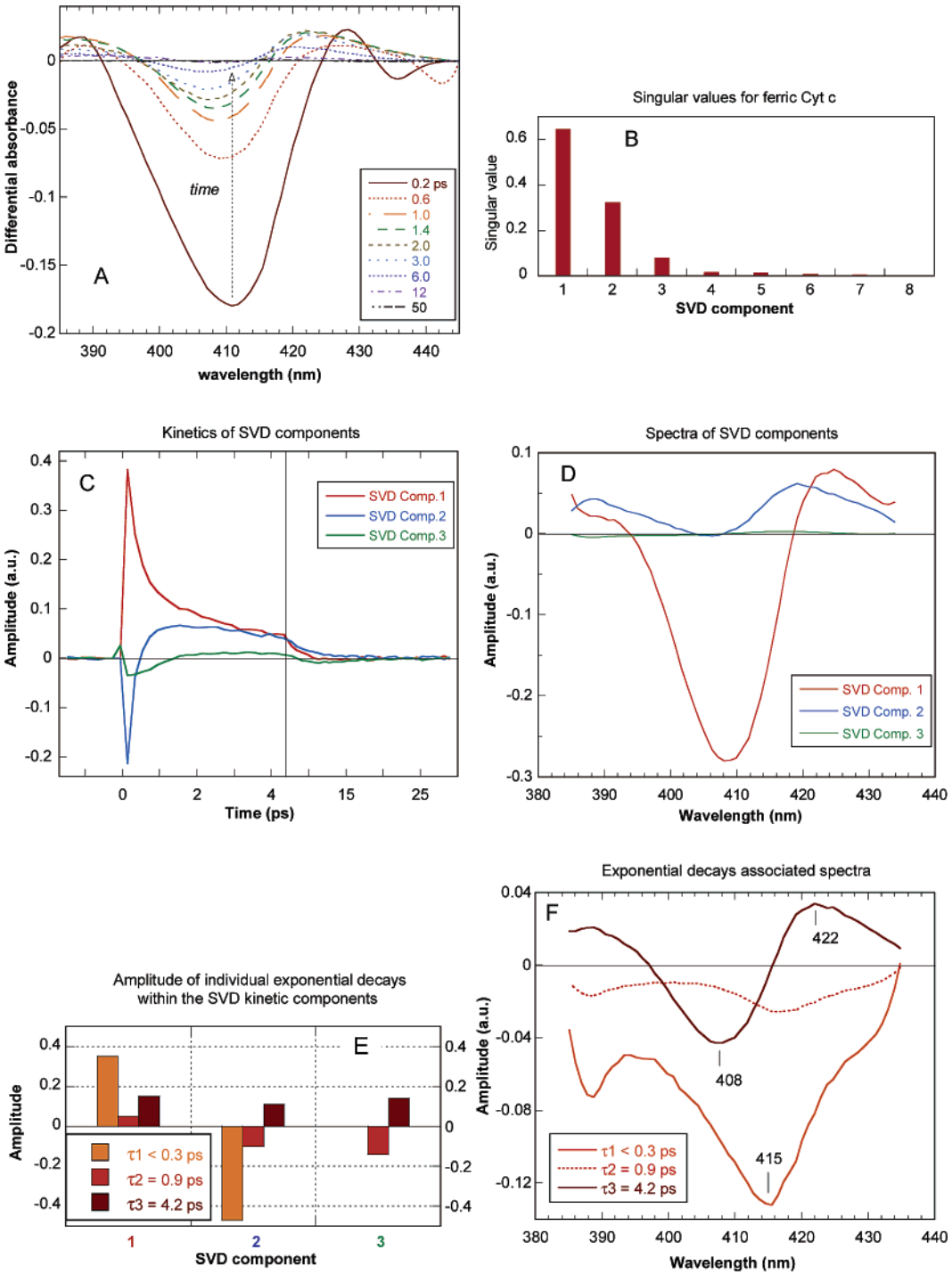

Figure 4. TA spectra of ferric Cyt *c*, in buffer pH 7.4, shown at several chosen time delays (panel A) and the results of SVD analysis (panels B−D) and fits of these components in terms of DAS (E,F). The earliest TA spectrum (panel A) and DAS spectrum (panel F) are contaminated by GVD effects outside of the 395−425 nm range. See text for details of data treatment.

that are shifted substantially with respect to their ground-state counterparts. In Figure 5, the pairs $\nu_4-\nu_4^*$ (1360 and 1345 cm^{-1}, respectively) and $\nu_3-\nu_3^*$ (1490 and 1453 cm^{-1}, respectively)[59] have been used for determining the value of factor *K*, which was varied from 0.6 at $\Delta t = 1$ ps to 0.93 at $\Delta t = 15$ ps.

Note, that for TR^3 spectra in the low-frequency range (see below, Figure 10), separation of the ground- and transient-state bands is less evident; thus, accurate determination of *K* factors is difficult. Therefore, for treatment of low-frequency spectra we applied the subtraction factors determined from TR^3 spectra in the high-frequency range, since the experimental conditions were the same in both cases.

The difference TR^3 spectra thus obtained (Figure 5C−L) represent pure scattering from the photoinduced state of ferrous Cyt *c*, without the ground-state contribution. Absence of the photoinduced features at $\Delta t = -1$ ps (Figure 2C) confirms that the time-resolution of our TR^3 spectrometer is better than 1 ps. New transient Raman bands appear immediately at positive time delays, with prominent peaks at $\Delta t = 1$ ps at 1345 cm^{-1} (ν_4^*), 1454 cm^{-1} (ν_3^*), and 1570 cm^{-1} (ν_2^*). As time elapses, these transient bands experience high-frequency shifts (1345 → 1352 cm^{-1}, 1453 → 1456 cm^{-1}, 1570 → 1576 cm^{-1}); also they decrease in intensity and at $\Delta t = 15$ ps almost disappear, along with the recovery of the ground-state scattering signal. This

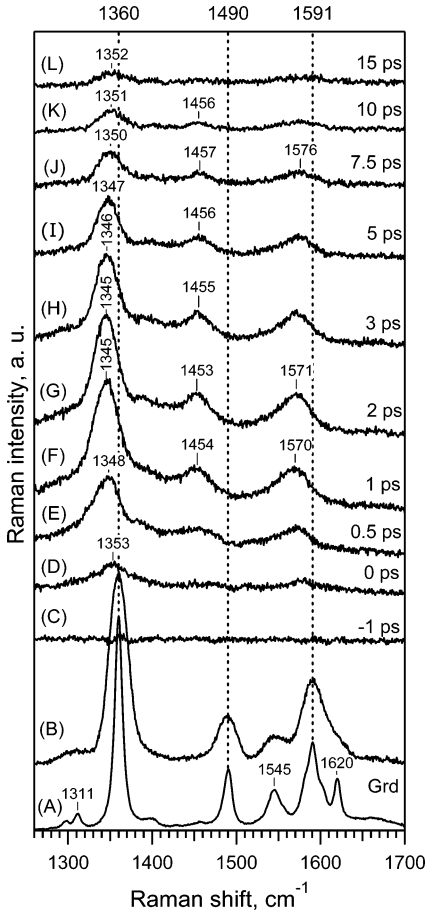

Figure 5. TR^3 spectra in the high-frequency range of ferrous Cyt *c*, in buffer pH 7.4. Spectra A and B are ground-state spectra recorded with cw excitation at 441.6 nm and with subpicosecond excitation at 435 nm, respectively. Spectra C−L are difference spectra at various Δt: −1 (C), 0 (D), 0.5 (E), 1 (F), 2 (G), 3 (H), 5 (I), 7.5 (J), 10 (K), and 15 ps (L). Accumulation time was 10 min for each spectrum.

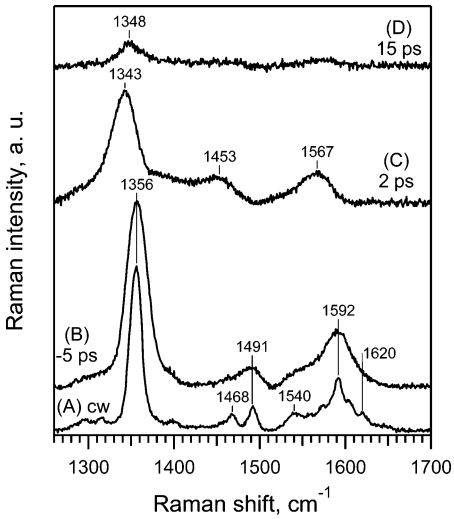

Figure 6. TR^3 spectra in the high-frequency range of ferrous Cyt *c* N-fragment, in buffer pH 9. Spectra C and D are difference spectra at $\Delta t = 2$ and 15 ps, respectively. Accumulation time was 30 min.

behavior is in a good agreement with our TA data (Figure 2) which showed that about 92% of absorption changes decays with time constants of ≤4.8 ps. It is interesting to note that the TR^3 spectrum at 7.5 ps (Figure 5J) reveals the same frequencies of the ν_2*, ν_3*, and ν_4* bands and also the overall bands

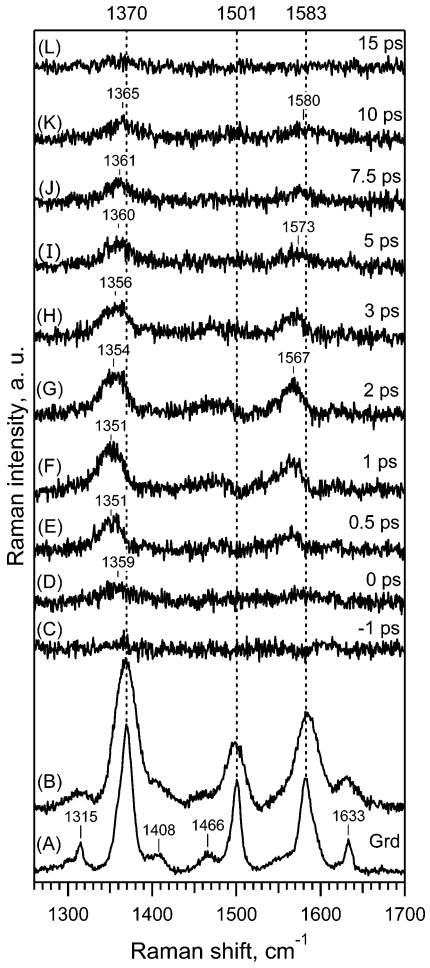

Figure 7. TR^3 spectra in the high-frequency range of ferric Cyt *c*, at pH 7.4. Accumulation time was 20 min.

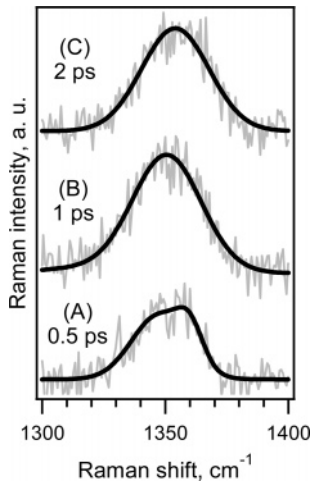

Figure 8. Expanded view in the ν_4*-band region of the difference TR^3 spectra of ferric Cyt *c* from Figure 7, obtained at $\Delta t = 0.5$ (A), 1 (B), and 2 ps (C). Thin gray lines denote experimental points, thick black lines correspond to the best-fit curves using Voigtian contours.

intensity distribution as in the difference spectrum obtained in resonance Raman saturation study utilizing 10-ns laser pulses (Figure 8 of ref 38).

Ferrous N-Fragment. Figure 6 presents TR^3 spectra in the high-frequency range of ferrous Cyt *c* N-fragment. The ground-state spectrum recorded with cw excitation (Figure 6A) is in agreement with the published one in the range 1450−1630 cm^{-1} (Figure 6b of ref 53) and represents scattering from the major

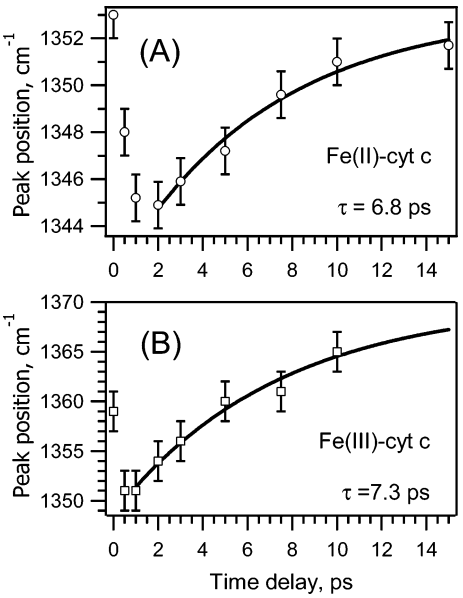

Figure 9. Peak position of transient ν_4*-band versus time for ferrous (A) and ferric (B) Cyt *c*. Markers denote frequencies of Voigtian contours, solid curves are the best fits by a single-exponential function with the following parameters: (A) $\tau = 6.8 \pm 2.1$ ps, offset 1353 cm^{-1}; (B) $\tau = 7.3 \pm 2.2$ ps, offset 1370 cm^{-1}.

6cLS form.[53] However, a minor contribution from the 5cHS species is also present judging from the appearance of low-frequency-shifted bands/shoulders at 1468, ~1572, and ~1605 cm^{-1}, in pairs to the bands at 1491 (ν_3), 1592 (ν_2), and 1620 cm^{-1} (ν_{10}) of the 6cLS form. Note that this small amount of five-coordinate N-fragment molecules is more readily detected in Raman (Figure 6A) than in absorption (Figure 1c) because of selective resonance enhancement with 441.6-nm excitation.

Interestingly, the ν_4 band of Cyt *c* N-fragment at 1356 cm^{-1} does not split (in contrast to ν_2, ν_3, and ν_{10}, Figure 6A) being rather symmetrical. Thus the frequency of the ν_4 band remains virtually the same for both coordination states (6cLS and 5cHS) of the heme. Exactly the same behavior was observed[60] in cw resonance Raman spectra of another Cyt *c* model compound, ferrous microperoxidase-8 (MP-8), which may exist in both five- and six-coordination states depending on solvent composition.

Thus, the spectral shape of the ground-state Raman spectrum of ferrous N-fragment at pH 9 is somewhat complicated by the contribution from the 5cHS form. However, given the predominance of the 6cLS bisHis ligated form in the ground state, the major part of the photoproduct molecules represents transient five-coordinate Fe−His complexes, while contribution of the photoproduct arising from the very minor ground-state 5cHS species can be considered as negligible.

We note the obvious similarity of the photoproduct spectra at $\Delta t = 2$ ps of native ferrous Cyt *c* (Figure 5G) and its N-fragment (Figure 6C), except for the small relative low-frequency shifts of the bands in the latter case. This fact implies that the photoinduced species resemble each other, in agreement with our previous low-frequency TR^3 data[51] and with our present TA data (Figures 2 and 3). At $\Delta t = 15$ ps, however, the transient ν_4* band at 1348 cm^{-1} in the difference TR^3 spectrum of Cyt *c* N-fragment (Figure 6D) is more intense than its counterpart at 1352 cm^{-1} in the spectrum of native Cyt *c* (Figure 5L). This fact can be explained by the difference in lifetimes of the long-lived transient species in these two cases.

Ferric Cyt c. Figure 7 presents TR^3 spectra of ferric Cyt *c*, treated in the same manner as described above for ferrous Cyt *c*. Again, the cw ground-state spectrum (Figure 7A) is in agreement with literature data,[2,58] and the subpicosecond ground-state spectrum (Figure 7B) proves the absence of any photo-induced perturbations due to the probe pulse in time-resolved experiment. The intensity distribution between the bands ν_2, ν_3, and ν_4 (1583, 1501, and 1370 cm^{-1}, respectively) is characteristic of a ferric 6cLS heme structure and differs from that in the ferrous heme where a strong ν_4 band dominates the spectrum (Figure 5A).

Transient bands in difference TR^3 spectra of ferric Cyt *c* appear immediately after photoexcitation and are shifted to lower frequency with respect to their ground-state values (Figure 7D,E). Also, transient scattering contains Raman bands (Figure 7D−L) that are weaker than in the case of ferrous Cyt *c* (Figure 5D−L). This can be explained by the rather weak photoinduced absorption at 435 nm (Figure 4A,F), the wavelength of the Raman probe, and therefore by less favorable resonance enhancement of Raman scattering from the photoproduct species.

Time evolution of the transient difference spectra of ferric Cyt *c* (Figure 7D−L) reveals a photoinduced behavior different from that of ferrous Cyt *c*. Indeed, the photoproduct bands ν_4* and ν_2* experience a progressing high-frequency shift with time, from 1351 cm^{-1} at $\Delta t = 1$ ps to 1365 cm^{-1} at $\Delta t = 10$ ps and from 1567 cm^{-1} at $\Delta t = 2$ ps to 1580 cm^{-1} at $\Delta t = 10$ ps, respectively (Figure 8F−J), approaching in the limit their frequencies in the ground state. We recall that, by contrast, for ferrous Cyt *c* the photoproduct bands frequencies do not approach their ground-state values at any time delay (Figure 5F−L).

ν_4 Peak Shifts.* To quantify this observation, we performed a spectral fit by Voigtian contours of the ν_4*-band region in difference TR^3 spectra for both ferric and ferrous Cyt *c*, at all measured time delays. As an example, the first three fitted contours for ferric heme are presented in Figure 8. At $\Delta t = 0.5$ ps, the ν_4*-band contour is asymmetrical and was fitted by 2 lines (Figure 8A).

Starting from $\Delta t = 1$ ps, spectral line shapes become more symmetrical and were fitted by a single Voigtian contour, although some deviation between the fit and the experimental data points is noticeable in the high-frequency edge of the contours. However, taking into account that spectral resolution of our TR^3 experiment is ~30 cm^{-1}, this deviation was considered as negligible. The accuracy in peak position determination was estimated to be ± 2 cm^{-1}.

The resulting time dependencies of Raman peak positions are presented by markers in Figure 9 for the photoproducts of ferrous (panel A) and ferric (panel B) Cyt *c*. The frequency of the ν_4* band initially decreases and then, at $\Delta t \geq 1-2$ ps, again increases, with the minimum around $\Delta t = 1.5$ ps for ferrous and around $\Delta t = 0.7$ ps for ferric Cyt *c*. A single-exponential fit has been performed, starting from $\Delta t \geq 2$ ps for ferrous and from $\Delta t \geq 1$ ps for ferric Cyt *c* (solid curves in Figure 9), and, within the experimental accuracy, the same time constant of ~7 ps was obtained for both Cyt *c* oxidation states.

However, the magnitude of the frequency shift is quite different: 8 cm^{-1} for ferrous and 19 cm^{-1} for ferric heme. Also, as noted above, the frequency of the transient ν_4* band of ferric Cyt *c* approaches (at $t \rightarrow \infty$) the ground-state value of 1370 cm^{-1}, while this is not the case for ferrous Cyt *c* where the limiting value of 1353 cm^{-1} is still shifted by 7 cm^{-1} from the ground-state position at 1360 cm^{-1}.

Spectra in the Low-Frequency Range. Finally, Figure 10 presents comparative TR^3 spectra in the low-frequency range, for Cyt *c* in both oxidation states of the heme. As reported

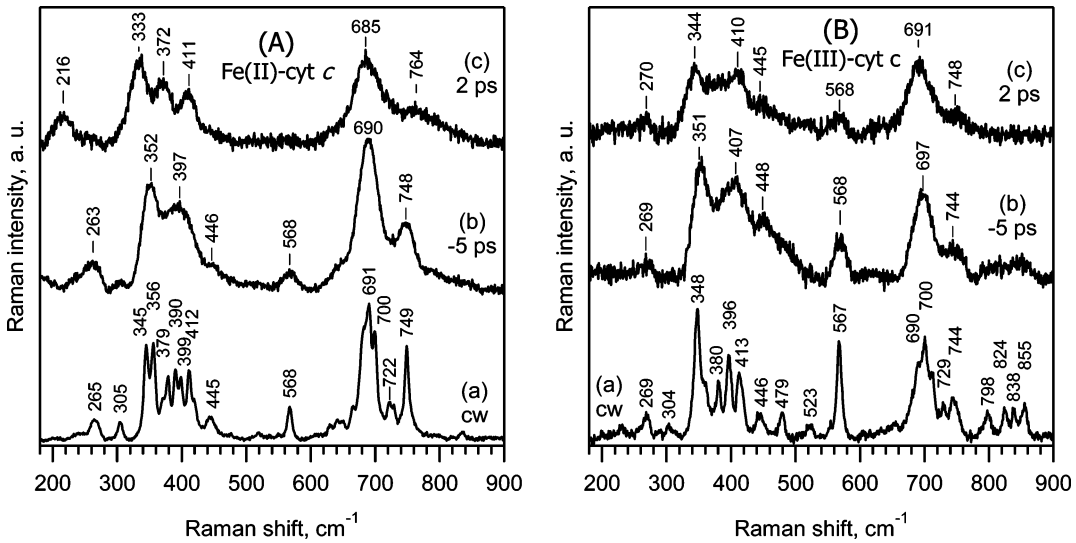

Figure 10. TR^3 spectra in the low-frequency range of ferrous (A) and ferric (B) Cyt *c*. Spectra a and b are ground-state spectra recorded with cw excitation at 441.6 nm and with subpicosecond excitation ($\Delta t = -5$ ps) at 435 nm, respectively. Spectra c are difference spectra at $\Delta t = 2$ ps.

previously,[51] for ferrous Cyt *c* the photoproduct spectrum at $\Delta t = 2$ ps (Figure 10Ac) is characterized by several pronounced spectral changes: (i) a new photoinduced band appears at 216 cm^{-1}; (ii) the complex unresolved contour in the ground-state spectrum around 397 cm^{-1} transforms into two separate bands at ~372 and ~411 cm^{-1}; and (iii) the prominent ground-state Raman band at ~568 cm^{-1} disappears in the photoproduct spectrum.

In contrast, photoinduced changes in transient TR^3 spectrum of ferric Cyt *c* (Figure 10Bc) are much less pronounced: the overall spectral patterns reveal substantial similarity with the ground-state spectrum (Figure 10Bb); and neither of the above-mentioned spectral changes for ferrous Cyt *c* is observed for ferric heme. The most noticeable difference in the latter case is the frequency shifts by 3−7 cm^{-1} of a number of bands. We note also that transient TR^3 spectra in the low-frequency range at $\Delta t = 2$ ps were found to be very similar for ferrous Cyt *c* and its N-fragment.[51]

Discussion

The results obtained in this study provide experimental evidence for various dynamic processes in Cyt *c*: electronic, vibrational and conformational relaxation, and axial ligand photodissociation and its subsequent rebinding. Below we discuss these specific contributions in detail for both oxidation states of the heme.

Methionine Photodissociation in Ferrous Cyt *c*. Our data fully support the reported[21,51] photolysis of methionine axial ligand from ferrous heme. The most direct evidence for Met-80 photodissociation is (i) the appearance, in transient difference TR^3 spectrum, of Fe−His band at 216 cm^{-1} (ref 51, Figure 10Ac) which is a well-known marker of five-coordinate domed heme structure[49] and (ii) close similarity of TA and TR^3 spectra of the photoproducts of initially different 6cLS species: His−Fe−Met in native Cyt *c* and His−Fe−His in Cyt *c* N-fragment. Other spectroscopic data are also in agreement with Met-80 photolysis: (i) the photoproduct species exhibits a characteristic derivative-like shape (DAS_3) associated with the dominant relaxation process $\tau_3 \approx 5$ ps, both in native ferrous Cyt *c* (Figure 2E,F) and in its N-fragment (Figure 3E,F); (ii) the porphyrin marker bands in the high-frequency range of transient TR^3 spectra experience low-frequency shifts with respect to their ground-state values (Figure 5,6) indicating expansion of the porphyrin macrocycle,[50] spin state change,[50] as well as vibrational heating (see below).

Concerning the photodissociation quantum yield, it was shown previously[21] that more than 80% of the excited molecules lose the methionine ligand, creating a five-coordinate photoproduct. Also, a femtosecond coherence spectroscopy study of Cyt *c*,[21] performed along with TA, allowed reconstruction of the vibrational mode at ~220 cm^{-1}, among others, which was interpreted as an iron−histidine vibration. Our data are fully consistent with the idea that Met-80 photolysis presents the major relaxation pathway in ferrous Cyt *c*.

Methionine Recombination. For native ferrous Cyt *c*, Met-80 rebinding is extremely rapid indicating that a five-coordinate photoproduct is energetically unfavorable. Two kinetic components could reasonably be assigned to recombination: a dominant component with $\tau_3 = 4.8$ ps and a minor component with $\tau_4 = 16$ ps; its relative weight is ~8%, well above the experimental accuracy (Figure 2E). The relaxation kinetics for the ferrous N-fragment, which possesses a compact structure different from the ordered secondary structure of native Cyt *c*, reveals a major "rapid" ($\tau_3 = 5.2$ ps) and two minor, "intermediate" ($\tau_4 = 30$ ps, weight ~7%) and "slow" ($\tau_5 > 1$ ns, weight ~7%) recombination phases. The latter phase is observed only for the truncated N-fragment structure.

It is important to stress that the dynamic processes associated with the 3rd (~5 ps) and 4th (16 or 30 ps) relaxation components originate from different transient states since the positions of isosbestic points in DAS_3 and DAS_4 differ by ~3 nm for both native Cyt *c* (Figure 2F) and its N-fragment (Figure 3F). At the same time, the 4th (30 ps) and 5th (∞) relaxation processes in the ferrous N-fragment originate from the same transient state as their isosbestic points and shapes coincide, and only the magnitude of absorption changes varies (Figure 3F).

Absence of Photolysis in Ferric Cyt *c*. The photophysical behavior of ferric Cyt *c* differs in many aspects from that of ferrous Cyt *c*. Summarizing all findings, we did not find any convincing signs of axial bond cleavage in six-coordinate oxidized Cyt *c*. The most compelling evidence of the absence of photolysis came from TA data: no prominent induced absorption comparable with the ground-state bleaching was found in the 390−400 nm spectral region (Figure 4A) where the maximum of the Soret band of five-coordinate ferric heme is located. Indeed, for 5cHS ferric configuration, the Soret band

maximum was reported at 398 nm for Cyt *c* and at 396 nm for Cyt *c′*, both at pH 0.3,[61] at 398 nm for FixL at neutral pH,[62] at 394 nm for Mb mutant H64L which lacks the sixth coordination with water,[63] and at 398 nm for eNOS[28] which is predominantly in the Cys-5cHS state.[64] Moreover, a strong maximum around 400 nm was reported at $\Delta t = 50$ ns in the TA spectrum of nitrosylated ferric Cyt *c* in nanosecond flash photolysis study;[65] this photoproduct can reasonably be interpreted as a transient five-coordinate complex.

Further proof of the absence of methionine photodissociation from ferric Cyt *c* was found in the transient Raman spectrum of ferric Cyt *c* in the low-frequency range (Figure 10Bc). Although the iron−histidine stretching mode is usually hardly seen for oxidized hemes,[66] so that its absence cannot serve as a reliable measure of coordination dynamics, the overall pattern of a difference 2-ps TR^3 spectrum of ferric Cyt *c* reveals substantial similarity with its ground-state counterpart (Figure 10Bb). This behavior is in striking contrast with spectral changes for ferrous Cyt *c* described above and in ref 51.

Before discussing the nature of this diverse photophysical behavior of Cyt *c*, we will first discuss the common process of vibrational relaxation, which takes place on the time scale of <10 ps in both oxidation states of the heme.

Vibrational Relaxation. The importance of vibrational cooling in the relaxation dynamics has long been recognized for large molecules in solution[67] including heme proteins[22] and model metalloporphyrins.[68] Conversion of an absorbed 530-nm photon into vibrational energy was estimated to increase the temperature of the heme by 460 K;[22] this local heat must be dissipated quickly into the surroundings. In the TA experiment, the "classic" signature of thermal relaxation involves broadened and red-shifted absorption bands that undergo spectral narrowing and blue shifting.[68] A distinctive manifestation of such a process is a time-dependent gradual blue shift of the isosbestic point in the difference TA spectrum.

Our TA spectra do reveal a time-dependent gradual blue shift of the isosbestic point in the first ∼10 ps for all three heme proteins studied (Figures 2A, 3A, and 4A and Figures 1S and 2S of Supporting Information). However, for ferrous Cyt *c* and its N-fragment, this shift is rather moderate (∼3 nm), whereas for ferric Cyt *c* it is much more pronounced (∼10 nm). This finding shows, first, that vibrational cooling substantially contributes to the relaxation dynamics and, second, that this contribution is larger for ferric heme. The latter fact corroborates the conclusion about the absence of ligand photolysis in ferric Cyt *c* so that the absorbed photon energy is fully transformed into heat, while for ferrous Cyt *c*, part of the energy is used to break the iron−methionine axial bond, thus the effect of vibrational heating is less pronounced.

Resonance Raman spectra are also very sensitive to vibrational heating and cooling. Raman frequencies change with temperature because of anharmonic coupling of modes having thermal populations.[69,70] For example, a frequency shift as large as 15 cm^{-1} was observed for the core size marker band ν_{10} of model nickel porphyrin in varying the temperature from 40 to 600 K.[70] Note that not only the frequency position but also the bandwidth of a Raman transition is temperature dependent. Concerning TR^3 spectra of heme proteins, high-frequency time-dependent shifts of the photoproduct marker bands have been reported for carbonmonoxy-Hb[24,36] and Mb[41] and interpreted as heme vibrational cooling.

Temperature changes have also been monitored by the ratio of Stokes to anti-Stokes Raman intensity[37,38] as well as by anti-Stokes Raman intensity kinetics.[41,42,47] Unfortunately, the relationship between Raman intensity and population of vibrational levels is not straightforward during the very first picoseconds after photoexcitation because of the complicated dynamic change in Raman resonance enhancement associated with spectral broadening and shift of the photoproduct absorption bands.[32] Since the major relaxation processes in Cyt *c* are very rapid, we focused namely on Raman frequency shifts rather than on Raman intensities.

The dependencies of ν_4* frequency versus time delay (Figure 9) contain two distinct regions: a steep declining phase leading to a minimum at ∼0.7 ps for ferric Cyt *c* and at ∼1.5 ps for ferrous Cyt *c* and a slower recovery part. This is the first instance when such a two-phase peak position shift is resolved for heme proteins (cf. ref 41 and ref 47), presumably because of sufficient temporal resolution (∼0.6 ps) in our TR^3 experiment. Remarkably, a very similar time-dependent alternating frequency shift with a slower decline phase has been previously reported for the extensively studied C═C stretch at 1570 cm^{-1} of singlet-excited *trans*-stilbene using longer several-ps laser pulses.[71−73] A linear correlation was obtained between temperature and Raman peak position[71,73] so that a Raman frequency shift was suggested to be a direct indicator of temperature change, serving as a so-called "picosecond Raman thermometer".[73]

Although vibrational cooling is not an exponential process, in the spirit of these previous studies, we have performed a phenomenological single-exponential fit to the peak position points at the relaxation part of the curves (Figure 9) and obtained, within the experimental accuracy, the same relaxation constant of about 7 ps for both oxidation states of the heme. This time constant should be considered an average estimate for the temperature decrease which appears to proceed with similar rates disregarding the heme iron oxidation state and the excess energy that must be dissipated. Note that interpretation of the ν_4* band shift, as large as ∼19 cm^{-1} in ferric Cyt *c*, by heme conformational changes as was suggested[40] for Hb and Mb seems less probable because the ν_4-band frequency is not particularly sensitive to the macrocycle distortions.[74]

Our results can be compared with molecular dynamics (MD) simulations for Mb and Cyt *c* on the energy flow from the heme into the surrounding protein matrix,[22] which predicted that vibrational cooling occurs on the ps time scale and that the temperature decay is nonexponential with about 50% decay occurring in 1−4 ps and the remainder in 20−40 ps. However, these calculations have been performed in vacuo, neglecting the important contribution from the solvated water molecules which may serve as an effective thermal sink. Further study of the problem from another "heat acceptor" perspective by fs IR spectroscopy of deoxy-Hb and Mb in D_2O[26] revealed water heating with a fast component of ∼8 ps and a slow component of ∼20 ps. To explain the fast component, which could not be described by classical diffusion theory, a spatially directed flow of energy through collective motions of the protein has been proposed.[26] Recent MD simulations[75] of photoexcited carbonmonoxy-Mb which took into account the solvent bath, have suggested that, after rapid equipartitioning of the excess energy in the heme moiety, further heme cooling proceeds predominantly by anisotropic energy "funneling" through the heme side chains to the surrounding water molecules according to an exponential process with a single time constant of ∼5.9 ps. No evidence was found[75] for substantially longer relaxation on the order of 20−40 ps in solvated protein that can be attributed to a classical diffusional energy transfer from the heme to the surrounding protein and subsequently to the solvent. This computational result is in agreement with a fs near-IR absor-

bance study of the band III of photoexcited Mb where the longest relaxation time constant of about 6 ps was obtained and interpreted as vibrational cooling of the electronically relaxed heme.[27] At the same time, classical molecular dynamics simulations from the same group on fully solvated Cyt *c* revealed a biphasic exponential decay process with time constants of 1.5 ps (weight ~60%) and 10.1 ps (weight ~40%).[76] The simulated difference in heme cooling between Mb[75] and Cyt *c*[76] was suggested to result from topological variations in heme/protein connectivity and variations in the accessibility of the heme to the water solvent. Finally, in a very recent overview of theories related to vibrational energy relaxation in proteins, it was emphasized that the accuracy of the force-field parameters is the most challenging problem since the calculated vibrational relaxation rate in Cyt *c* can vary by 2 orders of magnitude when the bond force constant is changed by only 10%.[77]

For ferric Cyt *c*, our data suggest that intermolecular vibrational relaxation proceeds in a single phase with a time constant of ~4 ps (TA decay) or ~7 ps (temperature decay) thus supporting the idea of the absence of classical heat diffusion from the heme into the surroundings. For ferrous Cyt *c*, it was suggested previously[21] that vibrational cooling proceeds in several steps with relaxation time constants ≤ 2.8 ps, while the 6.2 ps decay was attributed solely to methionine rebinding. However, temperature decay of ~7 ps, obtained from the ν_4* frequency shift in our TR^3 spectra, reveals that both axial ligand rebinding and intermolecular vibrational energy transfer occur on the same time scale. It is important to stress that the more long-lived TA decay components ($\tau \geq 16$ ps) for ferrous Cyt *c* (Figure 2E,F) and its N-fragment (Figure 3E,F) cannot be interpreted by vibrational relaxation. Indeed, $DAS_{4,5}$ exhibit a red-shifted isosbestic point with respect to DAS_3, that is in the opposite direction to what is expected in the case of vibrational cooling.

The above-described linear correlation between Raman peak shift and temperature was formulated in assuming Boltzmann statistics.[73] However, this is unjustified at the very early relaxation stages during which the initial excitation of the selected accepting vibrational modes is redistributing among all the heme intramolecular vibrations. For ferric Cyt *c*, the asymmetric spectral shape of the ν_4*-band contour at $\Delta t = 0.5$ ps (Figure 8A), steep decline and minimum in the ν_4*-peak position at ~0.7 ps (Figure 9B), and the second TA kinetic component $\tau_2 = 0.9$ ps (Figure 4E,F) can be associated with a nonequilibrium intramolecular vibrational energy redistribution (IVER) which eventually results in the equilibrated hot heme characterized by a Boltzmann temperature.[67] For ferrous Cyt *c*, the IVER seems to proceed more slowly: the ν_4*-peak position reaches its minimum at ~1.5 ps (Figure 9A), and the second TA kinetic component has a time constant $\tau_2 = 2.5$ ps (Figure 2E,F) with an associated spectrum of different shape. It is tempting to explain this effect by the influence of methionine photolysis on the IVER process. Although axial ligand photodissociation and subsequent central metal out-of-plane displacement take place immediately after excitation,[39,40] the resulting domed heme structure may somewhat perturb the IVER between the porphyrin modes. Interestingly, analogous contrasting cooling behavior has been reported[31] for 5cHS deoxy-Mb, as compared to vibrational cooling in the six-coordinated Mb-NO and Mb-O_2. However, it should be noted that DAS_2 in ferrous Cyt *c* (Figure 2F) is quite different from that in ferric Cyt *c* (Figure 4F), and the direct analogy of ultrafast relaxation processes in these two cases may not be completely valid.

Nature of Photoinduced Processes in Ferric Cyt *c*. At present time, there exists several models for interpretation of the ultrafast heme dynamics. Originally, the photoinduced changes in heme proteins have been interpreted by a series of electronic relaxations involving excited states of various origin.[23,24,36,44] Vibrational relaxation, although being acknowledged, was not considered as having a major contribution to relaxation dynamics.[23] An alternative model[21,29,31,32] is based on the immediate (in less than 1 ps) return of photoexcited heme into the hot ground state with subsequent vibrational cooling. According to this model, excited electronic states contribution is not required for interpretation of the available TA data on heme proteins. There exists also an "intermediate" approach in which contributions from both electronic and thermal relaxation were suggested on the time scale of 3−6 ps for interpretation of near-IR absorbance changes of the band III in photoexcited Mb.[27]

Our results on ferric Cyt *c* can be consistently explained using the vibrational relaxation model. The fastest TA decay ($\tau_1 <$ 0.3 ps), which is associated with a strong bleaching signal in the vicinity of the Soret-band maximum, is interpreted as a direct electronic relaxation to the hot ground state, possibly mixed with the very first stages of the IVER. The second TA kinetic component ($\tau_2 = 0.9$ ps) is associated with the IVER resulting in an equilibrated hot ground-state heme and possibly with a tail of the electronic relaxation. The asymmetric line shape of the transient ν_4* band at $\Delta t = 0.5$ ps and the minimum of the ν_4*-peak position dependence around ~0.7 ps support this assignment. The longest TA decay ($\tau_3 = 4.2$ ps) is ascribed to an intermolecular vibrational energy transfer from the hot heme to the surroundings, and the temperature decay of ~7 ps found from the ν_4* frequency shift confirms this interpretation.

We would like to stress again that, since vibrational relaxation is a nonexponential process, the exponential decay time constants discussed here must be considered just as guiding estimates. Thus, vibrational relaxation dominates photoinduced dynamics in ferric Cyt *c*. Experimental evidence that this process takes place essentially in the ground electronic state of the heme was found in TR^3 spectra: the photoproduct band frequencies approach in the limit their ground-state positions (Figure 7, 9). Although we cannot exclude completely a minor contribution from the excited electronic state relaxation, especially within the time range shorter 1 ps, our experimental data do not provide direct evidence of such a process.

Nature of Photoinduced Processes in Ferrous Cyt *c*. For ferrous Cyt *c*, the ultrafast heme dynamics is much more complicated than in the case of the ferric heme, with the methionine photodissociation and its subsequent rebinding being the dominant processes in the relaxation kinetics.

In the ground electronic state, the stability of the heme pocket of Cyt *c* is known to be greater in the reduced than in the oxidized form.[78,79] As an example, for ferric Cyt *c* at 59 °C, a temperature at which the protein is still folded, the methionine sulfur−heme iron bond was found to be already partially broken,[80] while for ferrous Cyt *c* no spectral changes can be detected[2] in the temperature range between 5 and 65 °C. Since for ferric Cyt *c* the methionine axial ligand is not photodissociated, we conclude that for ferrous Cyt *c* the sulfur−iron bond photocleavage takes place in the excited electronic state, not in the hot ground state of the heme.

Cyt *c* in both oxidation states possesses the same π-electron configuration of the heme macrocycle, and structural differences between the two states are very small.[79] Therefore, the mechanism of methionine photolysis must involve a dissociative

TABLE 1: Raman Frequencies of Porphyrin Marker Bands ν_4 and ν_3 at Different Heme Configurations for Ferrous Cyt *c* and Its Model Compounds

no.	ferrous compd	heme confign	ν_4 (cm^{-1})	$\Delta\nu_4$[a] (cm^{-1})	ν_3 (cm^{-1})	$\Delta\nu_3$[a] (cm^{-1})	ref
1	Cyt *c*	6cLS ground state	1360	7	1490	32	this study
		photoproduct	1353[b]		1458[b]		this study
2	Cyt *c* N-fragment, pH 9	6cLS ground state	1356	0	1491	23	this study
		5cHS ground state	1356[c]		1468		this study
3	Cyt *c* N-fragment, pH 7	6cLS ground state			1492	23	53
		5cHS ground state			1469		53
4	MP-8	6cLS ground state	1356	0	1492	24	60
		5cHS ground state	1356[c]		1468		60
5	Cyt *c* adsorbed on Ag electrode	6cLS ground state	1360	5	1491	24	2
		5cHS ground state	1355		1467		2

[a] Frequency difference between the two values from the preceding column. [b] Frequency values, determined by extrapolation of the experimental data trend $\nu = f(\Delta t)$ for $\Delta t \rightarrow \infty$. [c] Raman frequency of band ν_4^{5c} is indistinguishable from ν_4^{6c}.

excited state related to the d orbitals of the central metal as it is the number of d electrons that distinguishes ferric and ferrous heme. The nature of this state for ferrous Cyt *c* cannot be assessed from our TA and TR[3] data, as we did not detect a precursor six-coordinate transient species, and therefore the photolysis can be considered as instantaneous within our experimental time resolution. However, we can characterize the resulting five-coordinate photoproduct, which manifests itself both in TR[3] and TA spectra.

Photoproduct Raman Marker Band Frequencies. Transient difference Raman spectra originating from the photoproduct species are presented in Figure 5D−L. At early times, these spectra are heavily perturbed by vibrational relaxation as discussed above. However, at $\Delta t \geq 10$ ps, vibrational cooling is almost complete and we can obtain Raman frequencies of the thermally relaxed photoproduct by extrapolating the dependence $\nu = f(\Delta t)$ at $\Delta t \rightarrow \infty$. The first row of Table 1 presents these frequencies for the two most prominent Raman bands ν_4 and ν_3 of the photoproduct species (the ν_2-mode region is too crowded with bands and therefore is difficult to analyze with 30 cm^{-1} spectral resolution) in comparison with the frequencies of the six-coordinate ground-state species. The core-size marker band[50] ν_3 experiences a very large low-frequency shift by 32 cm^{-1} indicating substantial core expansion. The oxidation-state marker band[50] ν_4, which is also partially sensitive to core size and spin state, experiences a pronounced downshift of ~7 cm^{-1} in TR[3] spectra of both native ferrous Cyt *c* and its N-fragment. These low-frequency Raman band shifts are generally compatible with the creation of the 5cHS transient species and thus assigned to Met-80 photodissociation. However, direct comparison of Raman band shifts of the photoproduct species with those of the steady-state 5cHS species (rows 2−5 of Table 1) reveals important differences.

Although the stationary 5cHS configuration of native ferrous Cyt *c* in buffer solution is not available, several model compounds exist in this configuration that can be used for comparison. The distinctive feature of steady-state Raman spectra of a solution containing both 6cLS and 5cHS forms is the absence of the ν_4-band splitting, both for Cyt *c* N-fragment (Figure 6A) and for MP-8.[60] Therefore, we conclude that the ν_4-band frequency does not shift during the transition 6cLS → 5cHS in the ground electronic state in solution phase (rows 2 and 4, column 5), in contrast to the photoproduct case (row 1, column 5). At the same time, the ν_3 band of the ground-state 5cHS form does shift, by 23−24 cm^{-1} (rows 2−4, column 7), although this shift is smaller, by 8−9 cm^{-1}, than that in the photoproduct spectrum (row 1, column 7).

A slowly disappearing 5cHS configuration of ferrous Cyt *c*, in mixture with 6cLS, was obtained[2] electrochemically on a silver electrode from the conformational state II of ferric Cyt *c*, by changing the electrode potential from +0.35 to −0.25 V. The characteristic Raman frequencies of this 5cHS Cyt *c* species are presented in the 5th row of Table 1. A Raman shift of ~5 cm^{-1} for the ν_4 mode of the 5cHS form (row 5, column 5) is closer to that in the photoproduct spectrum; however, the ν_3-band shift of 24 cm^{-1} (row 5, column 7) is still distinctly different from the photoproduct case.

As a partial conclusion here, the analysis of Raman marker band frequencies suggests that the ferrous photoproduct species with the lifetime $\tau_3 = 4.8$ ps possesses a 5cHS structure different from that of the relaxed ground electronic state species.

For 6cLS ferrous hemes having two axial ligands, the configuration of d electrons of the central metal is $(d_\pi)^6(d_{z^2})^0(d_{x^2-y^2})^0$, and the core size of the porphyrin macrocycle is ~2.0 Å.[50] For 5cHS ferrous hemes having only one axial ligand, the d electrons' configuration is $(d_\pi)^4(d_{z^2})^1(d_{x^2-y^2})^1$, and the core size is ~2.4 Å.[50] Macrocycle expansion is required to accommodate an added electron density on the $d_{x^2-y^2}$ orbital and thus an increase of the in-plane electron radius of the central metal. Note that, for symmetry reasons, the d_{z^2} orbital occupation does not lead to a perturbation of the π-electron system of the porphyrin macrocycle. In steady-state Raman spectra of the 5cHS species of ferrous N-fragment, MP-8 and Cyt *c* adsorbed on a Ag electrode, this porphyrin core expansion is manifested by the 23−24 cm^{-1} low-frequency shift of the core-size marker band ν_3. Further frequency shift of this band in the photoproduct Raman spectrum may imply even larger core expansion. However, it should be noted that the core-size correlation is generally valid as long as the porphyrin structure is planar or preserves its degree of nonplanarity,[74,81] and this is obviously not the case for the transient photoproduct of ferrous Cyt *c*, which experiences important conformational changes.

Photoproduct Conformational Changes. Steady-state heme structure of horse heart Cyt *c* is essentially nonplanar, with the dominant distortions of ruffling and saddling types.[82] Structural consequences of photoinduced Met-80 detachment in ferrous Cyt *c* have been discussed in our previous study[51] on the basis of the photoproduct low-frequency TR[3] spectra. Transient heme distortions include (i) heme doming, coupled with the minor distortion of proximal His-18 side chain owing to the strain exerted by the protein as a result of iron out-of-plane displacement, (ii) change of the constraints in thioether links between two protoheme vinyl groups and side chains of two cysteine residues, and (iii) relaxation of steric constraints exerted by protein on the heme macrocycle, possibly due to the combined action of heme doming and alteration in coupling with cysteine residues. Indeed, the extent of porphyrin ruffling may diminish when the axial Met-80 ligand dissociates producing a doming

distortion. This process influences, in a complicated way, the frequencies of Raman marker bands[74] so that the extra low-frequency shift of $\sim 8-9$ cm^{-1} for the mode ν_3 can in principle be explained by the conformational changes of the photoproduct heme structure. However, the same line of reasoning seems less convincing for the frequency difference of ~ 7 cm^{-1} for the mode ν_4, because this mode is much less sensitive to the nonplanar macrocycle distortions as compared to ν_3.[74] Instead, the ν_4-band frequency is very sensitive to the electronic effects,[50] and therefore the excited electronic state contribution can also be suggested. As noted by the reviewer, for ferrous cyt *c*, an additional source of ν_4*-band shift could be changes in histidine hydrogen bonding and orientation, as well as interaction of dissociated methionine with the heme, affecting the antibonding heme π orbitals; this interesting possibility requires further investigation.

Photoproduct TA Spectra. Let us now consider the nature of the dynamic processes in ferrous Cyt *c* from the TA spectra. We start from the longest relaxation component with $\tau_5 \gg 1$ ns in ferrous Cyt *c* N-fragment (Figure 3E,F). At this time delay, all ultrafast electronic, vibrational, and conformational processes are already completed so that the relaxation can reasonably be ascribed to the coordination dynamics, namely to histidine rebinding for a population of the N-fragment which has undergone a structural rearrangement unfavorable for a direct histidine recombination. Accordingly, we assign the most long-lived transient species (τ_5, DAS_5) to the ground electronic state of the 5cHS form. Next, relaxation components τ_4 DAS_4 and τ_5 DAS_5 in ferrous N-fragment must originate from the same transient state since the isosbestic points and spectral shape of their DAS coincide and only the magnitude of absorption changes varies (Figure 3F).

The longest relaxation component for native Cyt *c* can also be assigned to the residual methionine recombination in the ground state of the 5cHS species. A plausible interpretation of this relatively long-lived ($\tau_4 = 16$ ps) minor recombination process assumes a small population of Cyt *c* for which a detached methionine side chain possesses a less favorable orientation with respect to the heme, so that steric hindrance exists for its rebinding already on the time scale of a few ps. This effect is even more pronounced in the case of histidine rebinding in the N-fragment, having a recombination component with $\tau_5 \gg 1$ ns. This is consistent with a more flexible structure of the N-fragment[52] as compared to native Cyt *c* and suggests that the protein secondary structure is important in preserving the stability of the six-coordinate complex.

At the same time, the third relaxation component τ_3 DAS_3, having a dominant contribution to the overall dynamics for both native Cyt *c* (Figure 2E,F) and its N-fragment (Figure 3E,F), belongs to the transient photoproduct state which is somewhat different from the 5cHS ground electronic state, corroborating TR^3 data discussed above. The blue shift of the isosbestic point by ~ 3 nm of DAS_3 with respect to DAS_4 and the general preservation of the spectral shape of DAS suggest that the dominant transient species with the lifetime τ_3 possesses an absorption spectrum similar to, but blue-shifted with respect to the spectrum of the 5cHS species in the ground electronic state.

Besides Met-80 recombination, conformational relaxation and excited electronic state decay may also take place on the time scale of the τ_3 process. Let us consider these two possibilities in more detail.

Nonplanar porphyrin macrocycle distortion causes the red shift of the optical absorption bands.[81] Consequently, as far as the conformational relaxation is concerned, the blue shift of DAS_3 with respect to DAS_4 is an evidence of the decrease of nonplanar heme distortion in the 5cHS transient species, probably due to a diminution of the heme ruffling in the domed five-coordinate structure. However, the absorption bands of metalloporphyrins are known to be only marginally affected by nonplanar distortions until the porphyrin atoms are displaced by more than 1 Å from the mean macrocycle plane (Figure 4 of ref 81). Since for horse heart Cyt *c* the dominant ruffled (average displacement of ~ 1 Å) and saddle (average displacement of ~ 0.2 Å) distortions do not exceed this value,[82] the decrease in the overall heme nonplanarity should not lead to a considerable shift of TA bands.

Optical properties of metalloporphyrin excited states have already been rigorously studied.[83] It was found that TA spectra of $\pi\pi^*$, $d\pi^*$ and dd excited states exhibit strong but not readily distinguishable absorption between the Soret- and Q-band bleachings,[83] all the excited-state bands being characteristically red-shifted with respect to their ground-state counterparts. At the same time, absorption spectra of the electrochemically prepared radical π cations exhibit a blue shift of the Soret-band maximum,[84] and spectral properties of the πd charge-transfer states should roughly resemble those of the ring radical π cation.[83] Resonance Raman spectra revealed that the mode ν_2, which is largely pyrrole $C_\beta C_\beta$ stretching, shifts up and down upon formation of the radical cation having a_{1_u} and a_{2_u} character, respectively, since the a_{1_u} orbital is antibonding and a_{2_u} is bonding with respect to the $C_\beta C_\beta$ bonds.[84] Therefore, taking into account the blue shift of the DAS_3 and the low-frequency shifts of all the photoproduct Raman marker bands (including ν_2), the participation of the excited πd charge-transfer state with the involvement of the porphyrin a_{2_u} orbital may be suggested.

The dynamic changes in TA spectra of ferrous Cyt *c* can also be considered from a slightly different point of view, namely, following the isosbestic point evolution (Figure 1S of Supporting Information), which is rather unusual. During the first ~ 7 ps, the isosbestic point shifts to the blue, from ~ 423 to ~ 420 nm, presumably reflecting the vibrational relaxation process.[68] However, at longer time delays, the isosbestic point position moves to the longer wavelengths, from ~ 420 nm at 7 ps to ~ 426 nm at ~ 50 ps. This red shift of ~ 6 nm is completely absent in the case of ferric Cyt *c* (Figure 2S of Supporting Information) and presumably reflects both conformational and electronic changes in the transient ferrous Cyt *c* species, as discussed above.

To obtain more information about the processes underlying this unusual red shift of the isosbestic point, we have performed an additional comparative TA study on ferrous complexes of Cyt *c* (Met-80 axial ligand), Cyt c(NO), and Mb(NO) under exactly the same experimental conditions. The pronounced red shift (~ 6 nm) of the isosbestic point in TA spectra in the time range $7-50$ ps has been confirmed for Cyt *c*(Met-80). A small red shift of ~ 1 nm has been found for Cyt *c*(NO). No shift at all has been detected after 12 ps for Mb(NO), corroborating previously published data.[31] These results are rather in favor of conformational relaxation hypothesis, although we cannot rule out completely the excited-state relaxation as well. Indeed, the electronic interaction of the heme iron with the methionine sulfur differs from that with the nitric oxide nitrogen, and the difference in the isosbestic point shift for Cyt *c*(Met) compared to Cyt *c*(NO) is rather large (6 versus 1 nm), in contrast to a rather small difference for Cyt *c*(NO) compared to Mb(NO) (1 versus 0 nm). The latter small difference in isosbestic point shift is undoubtedly related to the conformational difference between *b*- and *c*-type hemes. A comprehensive comparative study of

ferrous Cyt *c*(Met) and Cyt *c*(NO) is in progress, and the results will be reported in detail elsewhere.

Heme Dynamics in Ferrous Cyt *c*. Summarizing the discussion, we arrive at the following dynamic picture of the photoinduced processes in ferrous Cyt *c*. After absorption of a 550-nm photon due to $\pi\pi^*$ transition, ultrafast electronic relaxation takes place from the π system of the porphyrin ring to some unidentified dissociative excited-state involving d orbitals of central iron. Met-80 is released, and the system is placed in the hot transient 5cHS photoproduct state whose spectral characteristics are different from those of the relaxed ground-state 5cHS species. Further relaxation pathways include simultaneous vibrational cooling, conformational relaxation, and excited-state decay, coupled with the major phase of methionine back association to the heme iron. Since all these processes take place within the first 5−10 ps after photoexcitation, it is difficult to separate them unequivocally. Most probably, the first decay with $\tau_1 = 0.4$ ps has a dominant contribution from the excited-state relaxations mixed with the first stages of the IVER, the second decay with $\tau_2 = 2.5$ ps is primarily due to IVER in the excited state, and the third, dominating transient species with $\tau_3 = 4.8$ ps originates predominantly from Met-80 rebinding to the electronically and structurally distorted 5cHS photoproduct species, coupled with intermolecular vibrational energy transfer.

Concerning the longest relaxation component with $\tau_4 = 16$ ps for native Cyt *c*, which is minor (~8%) and which is assigned to methionine recombination in the ground electronic state of the 5cHS species, the following explanation could be suggested. In fact, although in steady state the Fe−methionine bond is rather strong in the ferrous state, methionine is not a very good axial ligand since thioether sulfur has negligible affinity for iron, for example, thioethers do not bind iron porphyrins.[79] Therefore, the otherwise weak methionine−iron interaction must be enhanced by favorable steric arrangement and low water content, two conditions that exist in native Cyt *c*.[79] Indeed, the microenvironment of the closed Cyt *c* crevice is hydrophobic, and Met-80 is normally placed in proper coordinating position by the protein fold. However, if heme doming due to methionine photolysis triggers a (rather slow) rearrangement of the whole protein structure then, after electronic relaxation in about 5 ps, some small amount of Cyt *c* molecules may already possess an unfavorable methionine−heme mutual orientation. As a result, methionine rebinding cannot proceed immediately, but some extra time is required to achieve a proper steric arrangement. This extra time is even longer for Cyt *c* N-fragment as it possesses a more flexible and opened structure. In this context, it is interesting to note that in the earlier TA study on ferrous six-coordinate deoxy-Dos,[9] more pronounced biexponential rebinding of the methionine ligand was observed with roughly equal amplitudes and time constants of 7 and 35 ps. As this protein ligand exchange between Met and external ligands has an important physiological function, we can speculate that a greater protein flexibility is at the origin of such prolonged rebinding kinetics, whereas Cyt *c* is very rigid which is more favorable for its main function as an electron-transfer protein.

Conclusions

On the basis of the results obtained in TR[3] and TA experiments and their joint analysis, the following main conclusions can be formulated:

(i) In ferric Cyt *c*, photodissociation of internal axial ligands to the heme iron does not take place, in contrast to the case of ferrous Cyt *c*.

(ii) In ferric Cyt *c*, the ultrafast heme dynamics is dominated by intramolecular vibrational energy redistribution (in less than 1 ps) with subsequent intermolecular vibrational energy transfer, in the ground electronic state of the heme. The latter vibrational relaxation proceeds in a single phase (time constant of ~4 ps in TA decay, ~7 ps in temperature decay), thus supporting the idea of the existence of a "doorway" for the anisotropic release of energy from the heme into the environment. An analogous ~7-ps temperature decay was observed for transient five-coordinate ferrous Cyt *c* species.

(iii) In ferrous Cyt *c*, dissociation of Met-80 is a major event after photoexcitation. Subsequent heme relaxation dynamics with $\tau \leq 5$ ps includes various simultaneous processes: excited electronic state decay, vibrational and conformational relaxations, and methionine recombination.

(iv) In ferrous Cyt *c*, the dominant relaxation process with $\tau = 4.8$ ps is assigned to the major part of Met-80 recombination to the 5cHS photoproduct species, which is structurally and electronically perturbed as compared to the corresponding relaxed ground electronic state species.

(v) In ferrous Cyt *c*, the minor more long-lived methionine recombination phase with $\tau = 16$ ps is assigned to a population of 5cHS Cyt *c* in the ground electronic state which does not have a favorable configuration for an ultrafast rebinding, following a slight change in protein structure induced by the methionine−iron bond cleavage. This long-lived recombination phase is even more pronounced in ferrous Cyt *c* N-fragment, which possesses a more flexible and opened structure.

Acknowledgment. This work was supported by a Marie Curie Training Site fellowship and a Boehringer Ingelheim fellowship to S.C. Grants from Fondation pour la Recherche Medicale, INSERM, and Ecole Polytechnique to S.G.K. are gratefully acknowledged. We thank P.-Y. Turpin for providing facilities for steady-state Raman measurements, J.-C. Lambry for technical assistance with time-resolved Raman setup, and S. Santucci for providing the Cyt *c* N-fragment.

Supporting Information Available: Two figures with shifts of the isosbestic points in TA spectra of ferrous and ferric cytochrome *c*. This material is available free of charge via the Internet at http://pubs.acs.org.

References and Notes

(1) Banci, L.; Assfalg, M. In *Handbook of Metalloproteins*; Wiley: Chichester, U.K. 2001; pp 33−43.

(2) Hildebrandt, P. In *Cytochrome c*: A Multidisciplinary Approach; Scott, R. A., Mauk, A. G., Eds.; University Science Book: Sausalito, CA, 1995; Vol. III, Chapter 6, pp 285−314.

(3) Banci, L.; Bertini, I.; Gray, H. B.; Luchinat, C.; Reddig, T.; Rosato, A.; Turano, P. *Biochemistry* **1997**, *36*, 9867−9877.

(4) Histidine 18 is named "proximal" by homology with other His-coordinated heme proteins such as myoglobin.

(5) Rogers, K. R. *Curr. Opin. Chem. Biol.* **1999**, *3*, 158−167.

(6) Lanzilotta, W. N.; Schuller, D. J.; Thorsteinsson, M. V.; Kerby, R. L.; Roberts, G. P.; Poulos, T. L. *Nat. Struct. Biol.* **2000**, *7*, 876−880.

(7) Yamamoto, K.; Ishikawa, H.; Takahashi, S.; Ishimori, K.; Morishima, I.; Nakajima, H.; Aono, S. *J. Biol. Chem.* **2001**, *276*, 11473−11476.

(8) Delgado-Nixon, V. M.; Gonzalez, G.; Gilles-Gonzalez, M. A. *Biochemistry* **2000**, *39*, 2685−2691.

(9) Liebl, U.; Bouzhir-Sima, L.; Kiger, L.; Marden, M. C.; Lambry, J. C.; Negrerie, M.; Vos, M. H. *Biochemistry* **2003**, *42*, 6527−6535.

(10) Stone, J. R.; Marletta, M. A. *Biochemistry* **1995**, *34*, 14668−14674.

(11) Negrerie, M.; Bouzhir, L.; Martin, J. L.; Liebl, U. *J. Biol. Chem.* **2001**, *276*, 46815−46821.

(12) Ishikawa, H.; Yun, B. G.; Takahashi, S.; Hori, H.; Matts, R. L.; Ishimori, K.; Morishima, I. *J. Am. Chem. Soc.* **2002**, *124*, 13696−13697.

(13) Schonhoff, C. M.; Gaston, B.; Mannick, J. B. *J. Biol. Chem.* **2003**, *278*, 18265−18270.

(14) Brzezinski, P.; Wilson, M. T. *Proc. Natl. Acad. Sci. U.S.A.* **1997**, *94*, 6176−6179.

(15) Silkstone, G.; Stanway, G.; Brzezinski, P.; Wilson, M. T. *Biophys. Chem.* **2002**, *98*, 65−77.

(16) Yoshimura, T.; Suzuki, S. *Inorg. Chim. Acta* **1988**, *152*, 241−249.
(17) Ascenzi, P.; Coletta, M.; Santucci, R.; Polizio, F.; Desideri, A. *J. Inorg. Biochem.* **1994**, *53*, 273−280.
(18) Kruglik, S. G.; Cianetti, S.; Vos, M. H.; Martin, J. L.; Negrerie, M., in preparation.
(19) Martin, J.-L.; Vos, M. H. In *Hemoglobins. Biophysical Methods*; Everse, J., Vandegriff, K. D., Winslow, R. M., Eds.; Methods in Enzymology, Vol. 232; Academic Press: San Diego, CA, 1994; pp 416−430.
(20) Jongeward, K. A.; Magde, D.; Taube, D. J.; Traylor, T. G. *J. Biol. Chem.* **1988**, *263*, 6027−6030.
(21) Wang, W.; Ye, X.; Demidov, A. A.; Rosca, F.; Sjodin, T.; Cao, W. X.; Sheeran, M.; Champion, P. M. *J. Phys. Chem. B* **2000**, *104*, 10789−10801.
(22) Henry, E. R.; Eaton, W. A.; Hochstrasser, R. M. *Proc. Natl. Acad. Sci. U.S.A.* **1986**, *83*, 8982−8986.
(23) Petrich, J. W.; Poyart, C.; Martin, J. L. *Biochemistry* **1988**, *27*, 4049−4060.
(24) Petrich, J. W.; Martin, J. L. *Chem. Phys.* **1989**, *131*, 31−47.
(25) Stoutland, P. O.; Lambry, J. C.; Martin, J. L.; Woodruff, W. H. *J. Phys. Chem.* **1991**, *95*, 6406−6408.
(26) Lian, T. Q.; Locke, B.; Kholodenko, Y.; Hochstrasser, R. M. *J. Phys. Chem.* **1994**, *98*, 11648−11656.
(27) Lim, M.; Jackson, T. A.; Anfinrud, P. A. *J. Phys. Chem.* **1996**, *100*, 12043−12051.
(28) Negrerie, M.; Berka, V.; Vos, M. H.; Liebl, U.; Lambry, J. C.; Tsai, A. L.; Martin, J. L. *J. Biol. Chem.* **1999**, *274*, 24694−24702.
(29) Kholodenko, Y.; Volk, M.; Gooding, E.; Hochstrasser, R. M. *Chem. Phys.* **2000**, *259*, 71−87.
(30) Liebl, U.; Bouzhir-Sima, L.; Negrerie, M.; Martin, J. L.; Vos, M. H. *Proc. Natl. Acad. Sci. U.S.A.* **2002**, *99*, 12771−12776.
(31) Ye, X.; Demidov, A.; Champion, P. M. *J. Am. Chem. Soc.* **2002**, *124*, 5914−5924.
(32) Ye, X. O.; Demidov, A.; Rosca, F.; Wang, W.; Kumar, A.; Ionascu, D.; Zhu, L. Y.; Barrick, D.; Wharton, D.; Champion, P. M. *J. Phys. Chem. A* **2003**, *107*, 8156−8165.
(33) Friedman, J. M. *Science* **1985**, *228*, 1273−1280.
(34) Findsen, E. W.; Friedman, J. M.; Ondrias, M. R.; Simon, S. R. *Science* **1985**, *229*, 661−665.
(35) Findsen, E. W.; Scott, T. W.; Chance, M. R.; Friedman, J. M.; Ondrias, M. R. *J. Am. Chem. Soc.* **1985**, *107*, 3355−3357.
(36) Petrich, J. W.; Martin, J. L.; Houde, D.; Poyart, C.; Orszag, A. *Biochemistry* **1987**, *26*, 7914−7923.
(37) Lingle, R.; Xu, X.; Zhu, H.; Yu, S.-C.; Hopkins, J. B.; Straub, K. D. *J. Am. Chem. Soc.* **1991**, *113*, 3992−3994.
(38) Li, P.; Sage, J. T.; Champion, P. M. *J. Chem. Phys.* **1992**, *97*, 3214−3227.
(39) Franzen, S.; Lambry, J. C.; Bohn, B.; Poyart, C.; Martin, J. L. *Nat. Struct. Biol.* **1994**, *1*, 230−233.
(40) Franzen, S.; Bohn, B.; Poyart, C.; Martin, J. L. *Biochemistry* **1995**, *34*, 1224−1237.
(41) Mizutani, Y.; Kitagawa, T. *Science* **1997**, *278*, 443−446.
(42) Kruglik, S. G.; Mizutani, Y.; Kitagawa, T. *Chem. Phys. Lett.* **1997**, *266*, 283−289.
(43) Uchida, T.; Ishikawa, H.; Ishimori, K.; Morishima, I.; Nakajima, H.; Aono, S.; Mizutani, Y.; Kitagawa, T. *Biochemistry* **2000**, *39*, 12747−12752.
(44) Franzen, S.; Kiger, L.; Poyart, C.; Martin, J. L. *Biophys. J.* **2001**, *80*, 2372−2385.
(45) Mizutani, Y.; Kitagawa, T. *J. Phys. Chem. B* **2001**, *105*, 10992−10999.
(46) Kruglik, S. G.; Mojzes, P.; Mizutani, Y.; Kitagawa, T.; Turpin, P. Y. *J. Phys. Chem. B* **2001**, *105*, 5018−5031.
(47) Mizutani, Y.; Kitagawa, T. *Chem. Rec.* **2001**, *1*, 258−275.
(48) Sato, A.; Sasakura, Y.; Sugiyama, S.; Sagami, I.; Shimizu, T.; Mizutani, Y.; Kitagawa, T. *J. Biol. Chem.* **2002**, *277*, 32650−32658.
(49) Kitagawa, T. In *Biological Applications of Raman Spectroscopy*; Spiro, T. G., Ed.; Wiley: New York, 1988; Vol. 3, Chapter 3, pp 97−131.
(50) Spiro, T. G. In *Biological Applications of Raman Spectroscopy*; Spiro, T. G., Ed.; Wiley: New York, 1988; Vol. 3, Chapter 1, pp 1−37.
(51) Cianetti, S.; Negrerie, M.; Vos, M. H.; Martin, J. L.; Kruglik, S. G. *J. Am. Chem. Soc.* **2004**, *126*, 13932−13933.
(52) Santucci, R.; Fiorucci, L.; Sinibaldi, F.; Polizio, F.; Desideri, A.; Ascoli, F. *Arch. Biochem. Biophys.* **2000**, *379*, 331−336.
(53) Santoni, E.; Scatragli, S.; Sinibaldi, F.; Fiorucci, L.; Santucci, R.; Smulevich, G. *J. Inorg. Biochem.* **2004**, *98*, 1067−1077.
(54) Teraoka, J.; Nakamoto, M. *J. Am. Chem. Soc.* **2000**, *122*, 6301−6302.
(55) Joffre, M.; Bonvalet, A.; Migus, A.; Martin, J. L. *Opt. Lett.* **1996**, *21*, 964−966.
(56) Vandegriff, K. D.; Shrager, R. I. In *Hemoglobins. Biophysical Methods*; Everse, J., Vandegriff, K. D., Winslow, R. M., Eds.; Methods in Enzymology; Academic Press: San Diego, CA, 1994; Vol. 232, pp 460−485.
(57) Press, W. H.; Flannery, B. P.; Teukolsky, S. A.; Vetterling, W. T. *Numerical Recipes*; Cambridge University Press: New York, 1989.
(58) Hu, S. Z.; Morris, I. K.; Singh, J. P.; Smith, K. M.; Spiro, T. G. *J. Am. Chem. Soc.* **1993**, *115*, 12446−12458.
(59) Raman bands assignment according to ref 2 and ref 58.
(60) Othman, S.; Le Lirzin, A.; Desbois, A. *Biochemistry* **1993**, *32*, 9781−9791.
(61) Indiani, C.; de Sanctis, G.; Neri, F.; Santos, H.; Smulevich, G.; Coletta, M. *Biochemistry* **2000**, *39*, 8234−8242.
(62) Gilles-Gonzalez, M. A.; Gonzalez, G.; Perutz, M. F.; Kiger, L.; Marden, M. C.; Poyart, C. *Biochemistry* **1994**, *33*, 8067−8073.
(63) Cao, W. X.; Christian, J. F.; Champion, P. M.; Rosca, F.; Sage, J. T. *Biochemistry* **2001**, *40*, 5728−5737.
(64) Schelvis, J. P. M.; Berka, V.; Babcock, G. T.; Tsai, A. L. *Biochemistry* **2002**, *41*, 5695−5701.
(65) Hoshino, M.; Ozawa, K.; Seki, H.; Ford, P. C. *J. Am. Chem. Soc.* **1993**, *115*, 9568−9575.
(66) Mitchell, M. L.; Li, X. Y.; Kincaid, J. R.; Spiro, T. G. *J. Phys. Chem.* **1987**, *91*, 4690−4696.
(67) Wondrazek, F.; Seilmeier, A.; Kaiser, W. *Chem. Phys. Lett.* **1984**, *104*, 121−128.
(68) Rodriguez, J.; Kirmaier, C.; Holten, D. *J. Chem. Phys.* **1991**, *94*, 6020−6029.
(69) Shelby, R. M.; Harris, C. B.; Cornelius, P. A. *J. Chem. Phys.* **1979**, *70*, 34−41.
(70) Asher, S. A.; Murtaugh, J. *J. Am. Chem. Soc.* **1983**, *105*, 7244−7251.
(71) Hester, R. E.; Matousek, P.; Moore, J. N.; Parker, A. W.; Toner, W. T.; Towrie, M. *Chem. Phys. Lett.* **1993**, *208*, 471−478.
(72) Qian, J.; Schultz, S. L.; Bradburn, G. R.; Jean, J. M. *J. Phys. Chem.* **1993**, *97*, 10638−10644.
(73) Iwata, K.; Hamaguchi, H. *J. Phys. Chem. A* **1997**, *101*, 632−637.
(74) Jentzen, W.; Simpson, M. C.; Hobbs, J. D.; Song, X.; Ema, T.; Nelson, N. Y.; Medforth, C. J.; Smith, K. M.; Veyrat, M.; Mazzanti, M.; Ramasseul, R.; Marchon, J. C.; Takeuchi, T.; Goddard, W. A.; Shelnutt, J. A. *J. Am. Chem. Soc.* **1995**, *117*, 11085−11097.
(75) Sagnella, D. E.; Straub, J. E. *J. Phys. Chem. B* **2001**, *1005*, 7057−7063.
(76) Bu, L. T.; Straub, J. E. *J. Phys. Chem. B* **2003**, *107*, 12339−12345.
(77) Fujisaki, H.; Straub, J. E. *Proc. Natl. Acad. Sci. U.S.A.* **2005**, *102*, 6726−6731.
(78) Margoliash, E.; Schejter, A. *Adv. Protein Chem.* **1966**, *21*, 113−283.
(79) Schejter, A. In *Cytochrome c*: A Multidisciplinary Approach; Scott, R. A., Mauk, A. G., Eds.; University Science Book: Sausalito, CA, 1996; Vol. IV, Chapter 8, pp 335−345.
(80) Taler, G.; Schejter, A.; Navon, G.; Vig, I.; Margoliash, E. *Biochemistry* **1995**, *34*, 14209−14212.
(81) Haddad, R. E.; Gazeau, S.; Pecaut, J.; Marchon, J. C.; Medforth, C. J.; Shelnutt, J. A. *J. Am. Chem. Soc.* **2003**, *125*, 1253−1268.
(82) Shelnutt, J. A.; Song, X. Z.; Ma, J. G.; Jia, S. L.; Jentzen, W.; Medforth, C. J. *Chem. Soc. Rev.* **1998**, *27*, 31−41.
(83) Rodriguez, J.; Kirmaier, C.; Holten, D. *J. Am. Chem. Soc.* **1989**, *111*, 6500−6506.
(84) Czernuszewicz, R. S.; Macor, K. A.; Li, X. Y.; Kincaid, J. R.; Spiro, T. G. *J. Am. Chem. Soc.* **1989**, *111*, 3860−3869.